

VYSOKÉ UČENÍ TECHNICKÉ V BRNĚ

BRNO UNIVERSITY OF TECHNOLOGY

FAKULTA ELEKTROTECHNIKY A KOMUNIKAČNÍCH TECHNOLOGIÍ
ÚSTAV VÝKONOVÉ ELEKTROTECHNIKY A ELEKTRONIKY

FACULTY OF ELECTRICAL ENGINEERING AND COMMUNICATION
DEPARTMENT OF POWER ELECTRICAL AND ELECTRONIC ENGINEERING

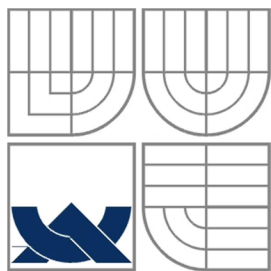
NÁVRH, OPTIMALIZACE A MODELOVÁNÍ PROVOZNÍCH STAVŮ SYNCHRONNÍHO STROJE S PERMANENTNÍMI MAGNETY NA ROTORU

DIPLOMOVÁ PRÁCE
MASTER'S THESIS

AUTOR PRÁCE
AUTHOR

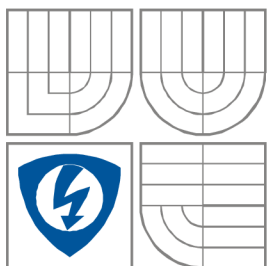
Bc.MARTIN BLÁHA

BRNO 2013



VYSOKÉ UČENÍ TECHNICKÉ V BRNĚ

BRNO UNIVERSITY OF TECHNOLOGY



FAKULTA ELEKTROTECHNIKY A KOMUNIKAČNÍCH TECHNOLOGIÍ
ÚSTAV VÝKONOVÉ ELEKTROTECHNIKY A ELEKTRONIKY

FACULTY OF ELECTRICAL ENGINEERING AND COMMUNICATION
DEPARTMENT OF POWER ELECTRICAL AND ELECTRONIC ENGINEERING

NÁVRH, OPTIMALIZACE A MODELOVÁNÍ PROVOZNÍCH STAVŮ SYNCHRONNÍHO STROJE S PERMANENTNÍMI MAGNETY NA ROTORU

DESIGN, OPTIMIZATION AND OF FULL LOAD CIRCUIT SIMULATION OF THE SURFACE
MOUNTED PERMANENT MAGNET MACHINE

DIPLOMOVÁ PRÁCE
MASTER'S THESIS

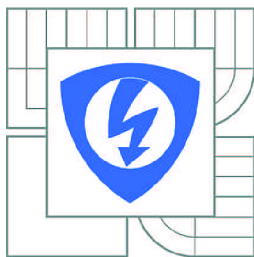
AUTOR PRÁCE
AUTHOR

Bc.MARTIN BLÁHA

VEDOUCÍ PRÁCE
SUPERVISOR

Ing.JIŘÍ KURFÜRST

BRNO 2013



VYSOKÉ UČENÍ
TECHNICKÉ V BRNĚ

Fakulta elektrotechniky
a komunikačních technologií

Ústav výkonové elektrotechniky a elektroniky

Diplomová práce

magisterský navazující studijní obor

Silnoproudá elektrotechnika a výkonová elektronika

Student: Bc. Martin Bláha

ID: 109633

Ročník: 2

Akademický rok: 2012/2013

NÁZEV TÉMATU:

Návrh, optimalizace a modelování provozních stavů synchronního stroje s permanentními magnety na rotoru

POKYNY PRO VYPRACOVÁNÍ:

1. Vytvořte parametrický model synchronního stroje s permanentními magnety na rotoru.
2. Na parametrickém modelu proveďte komplexní simulace magnetického obvodu naprázdno a při zatížení.
3. Teoreticky zpracujte možnosti využití optimalizačních algoritmů při návrhu elektrického stroje.
4. Proveďte optimalizaci vybraných parametrů stroje s ohledem na co nejlepší účinnost stroje při jmenovitém pracovním bodě.
5. Získané hodnoty porovnejte s původním strojem, který byl pro analýzu přidělen.

DOPORUČENÁ LITERATURA:

Dle doporučení vedoucího

Termín zadání: 17.9.2012

Termín odevzdání: 28.5.2013

Vedoucí práce: Ing. Jiří Kurfürst

Konzultanti diplomové práce:

Ing. Ondřej Vítek, Ph.D.

Předseda oborové rady

UPOZORNĚNÍ:

Autor diplomové práce nesmí při vytváření diplomové práce porušit autorská práva třetích osob, zejména nesmí zasahovat nedovoleným způsobem do cizích autorských práv osobnostních a musí si být plně vědom následků porušení ustanovení § 11 a následujících autorského zákona č. 121/2000 Sb., včetně možných trestněprávních důsledků vyplývajících z ustanovení části druhé, hlavy VI. díl 4 Trestního zákoníku č.40/2009 Sb.

Abstrakt

Tato práce pojednává o možnosti využití metody konečných prvků pro analýzu synchronního stroje s permanentními magnety na rotoru. Cílem této práce je ověření možnosti používat k efektivnějšímu návrhu synchronních motorů s permanentními magnety konečně prvkovou síť a software Maxwell. Na vytvořeném parametrickém modelu jsou provedeny simulace dle zadání. Cílem práce bylo zjištění indukovaného napětí, ztrát v železe, indukčností stroje, a provedení demagnetizační analýzy. Vytvořený parametrický model byl dále použit pro optimalizaci vybraných parametrů. Z výsledků optimalizace byly získány nové rozměry permanentních magnetů. Účinnost stroje byla zvýšena vlivem změny materiálu permanentních magnetů a optimalizovaných rozměrů stroje.

Abstract

This thesis deals with the possibility of using the finite elements method for the analysing of synchronous permanent magnets machines. The aim of this work is to discuss the possibility of the machine design more effectively with using the finite elements method and Maxwell software for the simulations. On the created parametric model, simulations were performed according to master thesis assignment. The aim of this work is to determine induced voltage, iron losses, machine inductances and make a permanent magnets demagnetization analysis. From simulations results the machine efficiency is calculated. The parametric model was used for the optimization of selected parameters. From results of optimization new dimensions of permanent magnets was obtained. Machine efficiency was increased by new permanent magnet material and optimized design.

Klíčová slova

Metoda konečných prvků ; Maxwell ; permanentní magnety ; synchronní stroj s permanentními magnety ; magnetická indukce ; ztráty v železe ; indukčnosti ; indukované napětí ; vinutí ; optimalizace ; SPEED ; demagnetizační analýza ; účinnost ; optimalizace

Keywords

Finite elements method ; Maxwell; permanent magnets ; synchronous machine with permanents magnets ; simulation ; flux density ; core losses ; inductances ; induced voltage; windings ; optimization ; Speed ; demagnetization analysis ; efficiency ; optimization

Bibliographic citation

BLÁHA, M. *Návrh, optimalizace a modelování provozních stavů synchronního stroje s permanentními magnety na rotoru*. Brno: Vysoké učení technické v Brně, Fakulta elektrotechniky a komunikačních technologií, 2013. 69s. Vedoucí diplomové práce Ing. Jiří Kurfürst.

Prohlášení(Statement)

Prohlašuji, že svou diplomovou práci na téma **NÁVRH, OPTIMALIZACE A MODELOVÁNÍ PROVOZNÍCH STAVŮ SYNCHRONNÍHO STROJE S PERMANENTNÍMI MAGNETY NA ROTORU** jsem vypracoval samostatně pod vedením vedoucího diplomové práce a s použitím odborné literatury a dalších informačních zdrojů, které jsou všechny citovány v práci a uvedeny v seznamu literatury na konci práce.

Jako autor uvedené diplomové práce dále prohlašuji, že v souvislosti s vytvořením této diplomové práce jsem neporušil autorská práva třetích osob, zejména jsem nezasáhl nedovoleným způsobem do cizích autorských práv osobnostních a jsem si plně vědom následků porušení ustanovení § 11 a následujících autorského zákona č. 121/2000 Sb., včetně možných trestněprávních důsledků vyplývajících z ustanovení § 152 trestního zákona č. 140/1961 Sb.

V Brně dne Podpis autora

Poděkování(Acknowledgments)

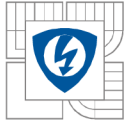
Děkuji vedoucímu diplomové práce **Ing. Jiřímu Kurfürstovi** za účinnou metodickou, pedagogickou a odbornou pomoc a další cenné rady při zpracování mé diplomové práce.

V Brně dne Podpis autora

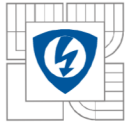


Summary

Summary	7
Index of figures	9
Index of tables	10
Nomenclature of used symbols	11
1 Introduction	14
2 Present status	16
2.1 MACHINE DESIGN FACTORS	16
2.2 THE TRADITIONAL MACHINE DESIGN APPROACH	16
2.2.1 <i>The sizing equation</i>	16
2.2.2 <i>Selection of the aspect ratio</i>	17
2.2.3 <i>Selection of current density</i>	17
2.2.4 <i>Selection of the flux density</i>	18
2.2.5 <i>Torque equations</i>	18
2.2.6 <i>The traditional electrical machine design process</i>	20
2.2.7 <i>Analytical model for the optimization</i>	21
3 Description of significant parameters of machine	22
3.1 BASIC GEOMETRY AND PARAMETERS OF SIMULATED MACHINE	22
3.2 DESCRIPTION OF THE BASIC STATOR PARAMETERS	24
3.3 DESCRIPTION OF THE BASIC ROTOR PARAMETERS	25
3.4 DESCRIPTION OF THE BASIC MAGNET PARAMETERS.....	25
3.5 DESCRIPTION OF THE BASIC WINDING PARAMETERS	26
3.6 CREATED PARAMETRIC MODEL.....	27
4 Selected simulations performed on parametric model	27
4.1 INDUCED VOLTAGE.....	29
4.2 COGGING TORQUE	32
4.3 EVALUATION OF THE STEADY TORQUE	35
4.3.1 <i>Load simulation in Rmxprt</i>	35
4.3.2 <i>Load torque characteristic</i>	36
4.3.3 <i>Load torque winding currents waveforms</i>	37
4.3.4 <i>Steady torque simulated on parametric model</i>	38
4.4 FLUX DENSITY DISTRIBUTION IN MACHINE GEOMETRY	39
4.4.1 <i>Radial flux density distribution in the air gap</i>	41
4.4.2 <i>Tangential flux density distribution in the air-gap</i>	42
4.5 IRON LOSSES.....	42
4.6 SOLID LOSSES	45
4.7 CALCULATION OF MACHINE INDUCTANCES	47
4.8 DEMAGNETIZATION ANALYSIS OF ORIGINAL NdFeB PERMANENT MAGNETS	51
4.9 CALCULATION OF THE MACHINE EFFICIENCY	54
5 Maxwell optimization analyses	55
5.1 GENETIC ALGORITHM.....	56
5.2 PATTERN SEARCH.....	56
5.3 QUASI NEWTON	56
5.4 SEQUENTIAL MIXED INTEGER NONLINEAR PROGRAMMING (SMINLP)	56

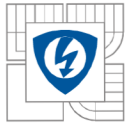


5.5	SEQUENTIAL NONLINEAR PROGRAMMING (SNLP).....	56
6	Performed optimization with respect to the highest possible efficiency	57
6.1	SELECTED OPTIMIZATION METHOD	57
6.2	PERFORMED OPTIMIZATION.....	57
7	Evaluation of optimization results, comparison with the original machine.....	58
	Conclusion.....	60
	References	63
	Appendix A1 (material properties of steel M19_24)	65
	Appendix B1 (material properties of NdFeB magnet)	67
	Appendix C1 (material properties of SmCo magnet).....	68



Index of figures

Fig 1.: Typical torque characteristics of an interior type permanent magnet motor.[8]	19
Fig 2.: Phasor diagram illustrating relation between stator fluxes and stator current. [12]	19
Fig 3.: Phasor diagram of vector controlled PM motor for maximum torque per stator current.[12] ..	20
Fig 4.: Machine geometry [19].....	23
Fig 5.: Stator slot geometry [19]	24
Fig 6.: Magnet parameters [19]	25
Fig 7.: Winding distribution in the slots.....	27
Fig 8.: Plotted mesh in the geometry of machine.....	28
Fig 9.: Plotted mesh3 in the geometry of machine.....	28
Fig 10.: Plotted mesh5 in the geometry of machine.....	29
Fig 11.: Induced voltage for simulation temperature 25°C,NdFeB magnets.	30
Fig 12.: Induced voltage for simulation temperature 125°C, NdFeB magnets.	30
Fig 13.: Induced voltage waveforms simulated at different temperatures, NdFeB magnets.....	31
Fig 14.: Induced voltage waveforms from different simulation software, NdFeB magnets	31
Fig 15.: Comparison of induced voltage waveforms using different permanent magnets material	32
Fig 16.: Cogging torque waveforms at different mesh conditions, 25°C, NdFeB magnets.	33
Fig 17.: Cogging torque waveforms at different mesh conditions, 125°C, NdFeB magnets.	34
Fig 18.: Cogging torque waveforms in different simulation conditions, NdFeB magnets.....	34
Fig 19.: Comparison of cogging torque waveforms using different permanent magnet material	35
Fig 20.: The torque waveform from simulation on model given by Rmxprt, NdFeB magnets.....	37
Fig 21.: Winding Currents.....	38
Fig 22.: Steady torque waveforms for two different permanent magnets material.	39
Fig 23.: Detail of saturation in teeth corners in no-load conditions	40
Fig 24.: Detail of saturation in teeth corners in load conditions.....	40
Fig 25.: Radial flux density distribution in the air gap.....	41
Fig 26.: Tangential flux density in the air gap.....	42
Fig 27.: Core losses waveform.	44
Fig 28.: Comparison of core losses waveforms using different magnet material	45
Fig 29.: Solid losses waveformss for NdFeB magnets.....	46
Fig 30.: Comparison of solid losses waveforms for both PM materials.....	46
Fig 31.: The waveforms of machine inductances.....	49
Fig 32.: Flux-linkage distribution in machine geometry for first-time simulation.....	49
Fig 33.: Flux-linkage distribution in machine geometry for condition $i_d=0$, $i_q=MAX$	50
Fig 34.: Flux-linkage distribution in machine geometry for condition $i_d=MAX$, $i_q=0$	50
Fig 35.: The second quadrant of demagnetization curve defines the basic parameters [16]	51
Fig 36.: Example of demagnetization characteristic for PM magnets at different temperatures [15]...	52
Fig 37.: Demagnetisation curves for magnet material ATMAXX33EH(NdFeB).....	53
Fig 38.: Power flow of PMSM[21].....	54
Fig 39.: PM dimensions from optimization.....	57
Fig 40.: BH curve of steel M19_24.....	65
Fig 41.: Properties of steel M19_24 in Maxwell.....	65
Fig 42.: Curves for calculation of core losses for steel M19_24 in Maxwell.....	66
Fig 43.: BH curve of magnet material ATMAXX33EH	67
Fig 44.: BH curve of magnet material YXG-28H	68



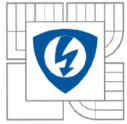
Index of tables

Table 3.1: Basic stator parameters.....	24
Table 3.2: Basic rotor parameters.....	25
Table 3.3: Basic magnet parameters.....	26
Table 3.4: Basic winding parameters	26
Table 3.5: Example of changing the magnet geometry by changing the parameter offsRmo.....	27
Table 4.1: Number of elements in selected meshes.....	28
Table 4.2: Cogging torque values at different simulation conditions for NdFeB magnets.	33
Table 4.3: Values of steady torque from parametric model simulation for both PM material.....	38
Table 4.4: Core losses values for different permanent magnet material.	45
Table 4.5: Values of solid losses.	47
Table 4.6: Input currents values	48
Table 4.7: Values of the calculated inductances.....	48
Table 4.8: Values for plotting the demagnetization curves	53
Table 4.9: Calculation of machine efficiency for different Pm material.....	54
Table 6.1: Values of parameters in performed optimization.....	58
Table 7.1: Results of performed optimization.....	59
Table 7.2: Values of steady torque for original and optimized design.....	59



Nomenclature of used symbols

Label	Description	Unit
A		
ac	Specific electrical loading	[A/m ²]
Awire	Cross sectional area of the copper wire	[mm ²]
B		
B _{fm}	Flux-density created by magnet	[T]
BetaM	Pole arc	[°e]
B _r	Remanent flux-density	[T]
\bar{B}	Specific magnetic loading	[T]
D		
D	Stator bore diameter	[mm]
δ	Torque angle	[°]
E		
E	Voltage	[V]
effa	Assumption of machine efficiency	[%]
EMF	Electro-magnetic field	
G		
Gap	Air-gap length	[mm]
H		
Hiperco	Name of the material	
I		
I	Current	[A]
InsThick	Layer insulation	[mm]
J		
J _s	Current density	[A/mm ²]
J _{RMS}	Current density per slot	[A/m ²]
K		
Kw1	Winding factor	

**L**

Lstator Length of stator [mm]

Lrotor Length of rotor [mm]

L Machine active length [mm]

λ Aspect ratio

Ld Inductance in d-axis [H]

Lq Inductance in q-axis [H]

Liner Slot liner [mm]

LM Length of magnet [mm]

LtL Line to line value

M

MIT Ministry of industry and trade

N

n Rated speed [rpm]

NSH Number of strands [-]

O

offset Coil pitch [-]

ω Angular velocity [rad.s⁻¹]

offsRmo Offset of arc radius Rmo [mm]

P

p Pole pairs [-]

Pem Maximum electromagnetic power [VA]

pfa Power factor [-]

PMSM Permanent magnet synchronous motor

PM Permanent magnet

Pk2pk Peak to peak value

PPath/2 Parallel branches [-]

R

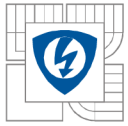
Rad2 Radius to the stator slot bottom [mm]

Ryoke Thickness of the rotor yoke [mm]

RadSH Shaft radius [mm]



Rad1	Rotor surface radius	[mm]
Rad3	Largest radius in the motor cross-section	[mm]
Rmo	Circular arc radius of outer face of the magnet	[mm]
RMS	Root-mean-square value	
S		
SD	Slot depth	[mm]
SO	Slot Opening	[mm]
SOAng	Slot opening angle	[°]
Syoke	Radial thickness of the stator yoke	[mm]
S	Motor rating from efficiency	[W]
Seff	Fill factor	
SFn	Limited fill factor	[-]
SUMMITOMO	Name of the material	
T		
Te	Electro-magnetic torque	[Nm]
TGD	Tooth edge length in vertical axis	[mm]
Tph	Conductor per slot	[-]
TWS	Tooth width	[mm]
V		
V	Phase applied voltage	[V]
W		
W _s	Medium slot width	[mm]
wMag	Width across one magnet	[mm]
WireDia	Wire size	[-]
X		
Xd	Reactance in d-axis	[Ω]
Xq	Reactance in q-axis	[Ω]



1 Introduction

This text was written as a master thesis. The aim of this study was to gain insight and understand methods that are used for the simulation, the optimization and the analysing of electrical machines.

This work discusses about the use of the finite elements method in the design of electrical machines. Finite element method is increasingly used as a tool for the design of a various technical device or their components. The main aim of this work is to use the finite element method for the analysis and the specific simulation of the synchronous machine with the surface mounted permanent magnets on the rotor. In order to properly evaluate the results of the simulations original motor was chosen. The specific simulations were already chosen in order to properly evaluate the results of the original designed machine.

This machine was studied in one of the projects opened by ministry of industry and trade (MIT). In recent years price of Neodymium-Iron-Boron (NdFeB) magnets was increased. For this reason the material of permanent magnets was changed for purpose of this master thesis. New material of permanent magnets was chosen with regard to the efficiency and price of the machine. Samarium-Cobalt (SmCo) was chosen from the permanent magnets materials.

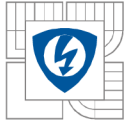
This work is divided into several chapters. The first chapter deals with traditional machine design approach. Permanent magnet synchronous machines are increasingly used in many industry applications. This is a main reason why this type of synchronous motor studying many experts in various projects. Whole chapter deals with basic equations and procedures to proper design of Permanent Magnet Synchronous Machine (PMSM) for each application.

The second chapter shows basic parameters and geometry of simulated machine. Parameters of stator, rotor, magnets, are described in this chapter. The geometry of machine is shown in figures. In geometry of machine, the main geometric parameters are identified. These identified parameters are important for creating of parametric model.

Software from Ansoft electromagnetic products was chosen as a simulation tool. Ansoft Maxwell 14 is complex simulation software for design, simulation and optimization of electric motors. Maxwell uses finite elements method for simulation. The Rmxprt is one of the Maxwell's plugins. Rmxprt is very good tool for electric machine simulations. In libraries are most types of electric machines. User selects his type of machine, sets required parameters and starts simulation. Rmxprt evaluate the results and displays them to the user. The big disadvantage of Rmxprt is low accuracy of the simulated model, but Rmxprt is very user-friendly.

Parametric model with using scripting was created for better accuracy. Parametric model respects all geometry parameters of proper machine. The properly created parametric model of the machine is important for correct evaluation of performed simulations. Individual parameters were used for creating a script in visual basic. With this script the user can very easily change geometry of the machine. Main advantage of this parametric model is possibility to do optimization cycles very easy.

The third chapter shows results of performed simulations on parametric model and their evaluation. Aim of this chapter is to determine properties of simulated machine. In this chapter the condition for each type of simulation are described. For proper evaluation of machine parameters three types of finite-element network are used. The impact on the accuracy of results, depending on the time of calculation and finite element network density, was investigated.



To verify the accuracy of parametric model, results were compared with results from other simulation software, where the same machine was simulated in project MIT.

For the comparison, the induced voltage waveforms from SPEED software were evaluated. From results, the accuracy of parametric model was confirmed. Waveforms of induced voltage for different simulation condition were evaluated.

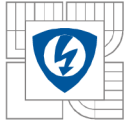
In next simulations, the value of steady torque is evaluated for both PM materials. From Rmxprt model, load torque curve was evaluated. Cogging torque waveforms are shown in figures and compared for different finite element networks densities and temperatures.

In next subchapter, flux density distribution in machine geometry is shown. Values of radial and tangential flux density in the air gap are calculated. Waveforms of core and solid losses are obtained and shown in figures for both PM materials. For correct identification of the machine, inductance values in dq coordinate system are calculated. For original NdFeB magnets, the demagnetization analysis is performed. Proper design of magnets is verified by demagnetization analysis.

For all simulation results the efficiency of the machine was calculated. Comparison between both PM materials is also described.

In next chapter, all Maxwell optimization methods are described. Advantages or disadvantages of each method are reviewed. For this master thesis, the generic algorithm is selected. Optimization of PM dimensions by generic algorithm is evaluated. Manual optimizations are also done. From optimization results, the new dimensions of PM are evaluated.

For new PM dimensions, the machine efficiency is calculated and evaluated. Evaluation of results obtained from all simulations and optimizations is performed in conclusion.



2 Present status

Growth in the use of synchronous machines, for a small and medium power, began with the use of permanent magnets manufactured from special alloy with high magnetic induction. Synchronous motors with these magnets (PMSM-Permanent Magnet Synchronous Motor) are regularly used in servomechanism, robotics and automation technology for over 10 years. PM synchronous motors are used in drives with outputs from hundreds of watts to tens of MW. In these areas, PMSM are replacing especially DC and stepper motors. In these days the trend is to use the PMSM in all possible applications. For each specific application, the machine must be carefully designed and constructed. [1], [2].

2.1 Machine design factors

Machine design is influenced by the following factors:

- Economics. Typically, machines are to be designed to have a minimum material cost and manufacturing cost. On the other hand, the trade-off between capital cost and operational cost should also be considered, especially for large machines, [1].
- Material limitations. The physical limits of materials generally determine the performance and dimensions of the machine, [1].
- Specifications and standards. In some applications, special considerations may exist that dominate the design. For example, aerospace motors require a design of minimum weight with maximum reliability. For the design of traction motors the emphasis is usually on reliability and the ability to satisfy a torque-speed curve. [1]

2.2 The Traditional Machine Design Approach

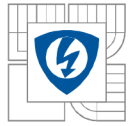
The traditional design approach was established nearly half a century ago and is dominated by rules of thumb and empirical curves that reflect the experiences of manufacturers, sometimes passed down from generation to generation as the established „company policy” way of doing it. In the traditional design, designers start by heuristically. Selecting values of design parameters, and then follows an iterative tuning process trying to achieve design specifications. [1]

2.2.1 The sizing equation

Traditional machine design usually starts from the famous sizing equation (2.1). [10]

$$S = 11K_{w1} \cdot \bar{B} \cdot ac * \left(\frac{D}{1000}\right)^2 * \frac{L}{1000} * n \quad (2.1)$$

where S is the motor rating in W, \bar{B} is the specific magnetic loading in Tesla, ac is the specific electrical loading in A/m, D is the stator bore diameter in millimetres, L is the generator active length in millimetres, K_{w1} is the winding factor for the fundamental, and n is the rated speed in rpm (revolutions per minute). Values for \bar{B} and ac are selected by the designer at the start of the design process.



The magnetic loading \bar{B} is limited by the saturation point of the materials used, the hysteresis losses and eddy current losses, the stray losses, the effectiveness of the cooling strategy, the load profile, and the duty cycle. The specific electric loading ac is limited by the copper loss in the conductors, the effectiveness of the cooling strategy, the temperature limitation of the insulation material, the load profile, and the duty cycle. In the traditional design, the selection of \bar{B} and ac is primarily based on the designer's experience. [1], [5]

2.2.2 Selection of the aspect ratio

After the selecting of the values of \bar{B} and ac , the D^2L value of the machine is then calculated by (2.2). For a machine with its pole number denoted by p , an aspect ratio λ is defined as:

$$\lambda = \frac{L}{(\pi \cdot D)/p} = \frac{L}{Y} \quad (2.2)$$

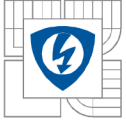
Where Y is the pole pitch in meters. By choosing a proper value for λ , D and L can be then calculated. Besides, \bar{B} , ac and λ are other design parameters that designers usually choose at the beginning of the design process. A good choice of λ helps to increase winding induced EMF with less coil length. With the same flux density, the induced EMF is proportional to the coil area. For highest induced EMF with the same coil length, the design of a rectangular coil shape with $\lambda = 1$ is desired. Besides this consideration, the selection of λ also depends on other factors, such as machine performance requirements, material consumptions, manufacturing feasibility and cooling. In the traditional design, the selection of the aspect ratio is also guided by empirical curves.[1]

2.2.3 Selection of current density

By selecting values for \bar{B} , ac and λ , another important design parameter to select is the stator current density J_s . For a certain rated current I , the current density J_s determines the cross sectional area of the copper wire A_{wire} used [3]:

$$A_{wire} = \frac{I}{J_s} \quad (2.3)$$

Higher current density leads to smaller A_{wire} and then larger armature resistance. For the same stator current, the copper loss is increased. This higher copper loss not only leads to lower machine efficiency, but also increases the winding operating temperature because more heat is generated. Since the winding operating temperature is limited by the maximum allowable temperature of the insulation, the machine designer should select a current density low enough that the operating temperature is within limits. On the other hand, when thinner wire is used, with the same number of winding turns, the amount of copper is reduced and less slot space is required to fit the wires. Accordingly, the teeth length can be reduced and the amount of steel is also reduced. The overall effect then leads to a reduction of the machine material cost and weight, which means that current density, should not be too small in order to avoid a bulky machine. In the traditional design, the current density is typically selected by rule of thumb or the designer's experience. According to certain empirical rules, the current density is generally selected in the range of 3 to 7,5 A/mm². In the traditional approach, many important factors in determining the temperature rise of machines cannot be easily taken into account, such as the ambient operating temperature, the available effective surface area for heat rejection, and the duty cycle of operation. However, a machine designed to run continuously under full load with a 40°C ambient temperature is expected to have much lower current density than a machine designed to



run intermittently and at an ambient of 10°C. In the traditional design, selecting the current density for both cases usually depends on a designer's experience and safety margin, which may often lead to over- or under-design of the electrical machines.[1]

2.2.4 Selection of the flux density

To fully utilize the material, the flux densities in the teeth and cores are usually selected around the knee point of the B-H curve. The traditional design rules were mostly developed based on silicon steel with a knee flux density around 1.4 T. However, with the improvement in magnetic material over the decades, core materials with saturation flux densities as high as 2,2 T have been produced, such as 'Hiperco' from Carpenter steel for example. Higher working flux density leads to smaller tooth width, thinner core, and thus smaller machines with the same rating. As a result, the empirical design curves that are based on a knee point of 1,4 T are inappropriate for machine designs using more modern magnetic materials.[1] [4]

2.2.5 Torque equations

Relationship between inductances in dq axes L_q, L_d and also the load angle δ_0 must be known, for the solving of torque equation. Since permanent magnets usually have a relative permeability close to that of the free space, for an interior-type PM motor the magnet thicknesses appear as large-series air gaps in the d-axis magnetic flux paths. The q-axis magnetic flux can pass through the ferromagnetic pole pieces without crossing the magnet and therefore the stator phase inductance is noticeably higher with q-axis rotor orientation. One of the most important consequences of having $L_d < L_q$ can be seen in the torque versus torque angle characteristic.

The equation of electro-dynamic torque is:

$$T_e = \frac{3p}{\omega} \left[\frac{E_0 V}{X_d} \cdot \sin \delta + \frac{V^2}{2} \left(\frac{1}{X_d} - \frac{1}{X_q} \right) \sin 2\delta \right] \quad (2.4)$$

Now we can write the equation (2.4) in this form:

$$T_e = T_{e1} \sin \delta + T_{e2} \sin 2\delta \quad (2.5)$$

Where the classic torque T_{e1} is:

$$T_{e1} = \frac{3pE_0V}{\omega X_d} \quad (2.6)$$

And the reluctance torque is:

$$T_{e2} = \frac{3pE_0^2}{2\omega} \left(\frac{X_q - X_d}{X_d X_q} \right) \quad (2.7)$$

Compared with a conventional synchronous motor, for which $X_d > X_q$ the reluctance torque T_{e2} is reversed in sign. It implies that at normal supply voltage, the total torque can be negative between $\delta = 0$ and $\delta = \delta_0$ as indicated in Fig 1 and since $\delta = 0$ is generally an unstable point, the no-load operation of a PM motor is at $\delta = \delta_0$. [8] [6]

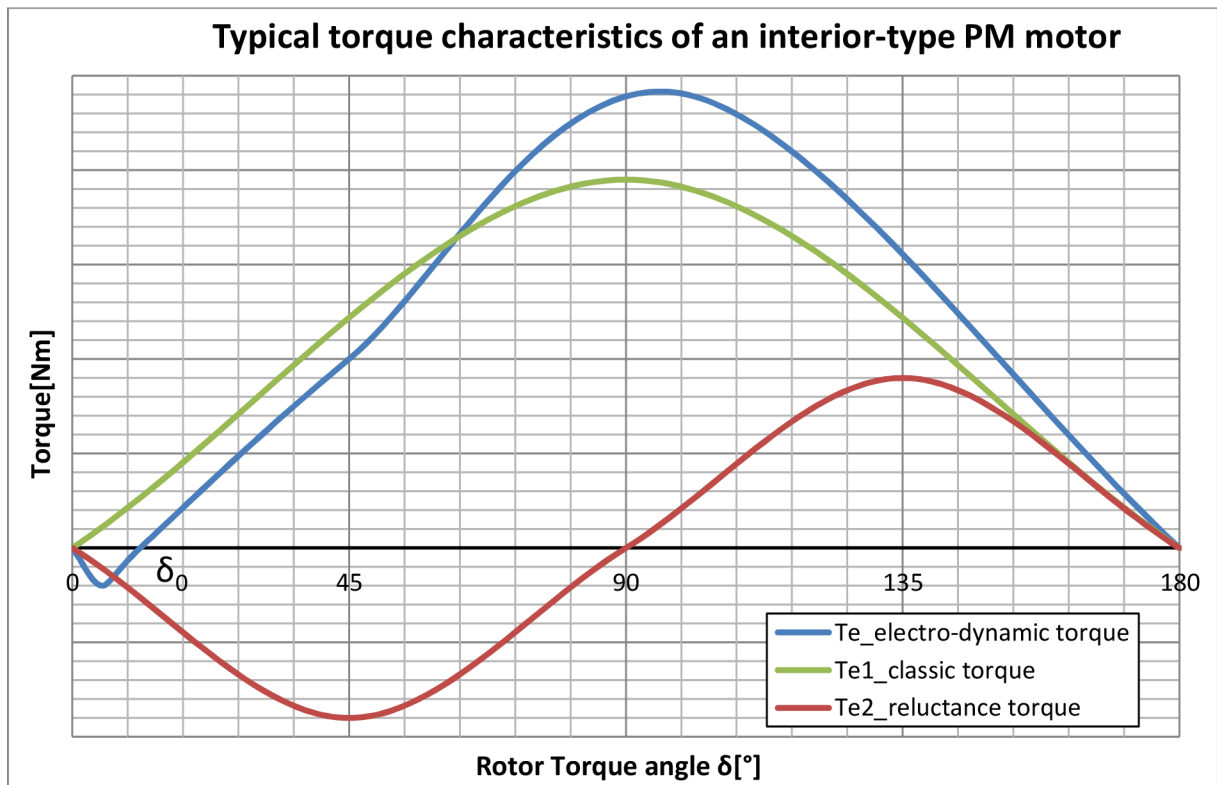
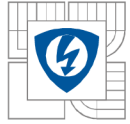


Fig 1.: Typical torque characteristics of an interior type permanent magnet motor.[8]

Phasor diagram of PM vector controlled machine is shown in Fig 3. For this case is value of load angle δ_0 set to achieve the maximum torque. Angle δ , called the torque angle, is the angle between the vector of stator current I_s and the direct axis which is aligned with the vector of the permanent magnet flux on the rotor. As it can be seen in Fig 2, the magnitude of the total stator flux depends on the location and magnitude of the stator current phasor. [12]

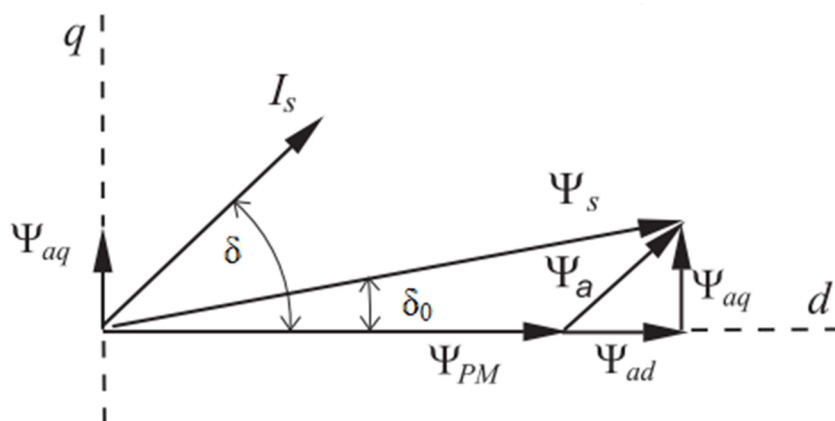


Fig 2.: Phasor diagram illustrating relation between stator fluxes and stator current. [12]

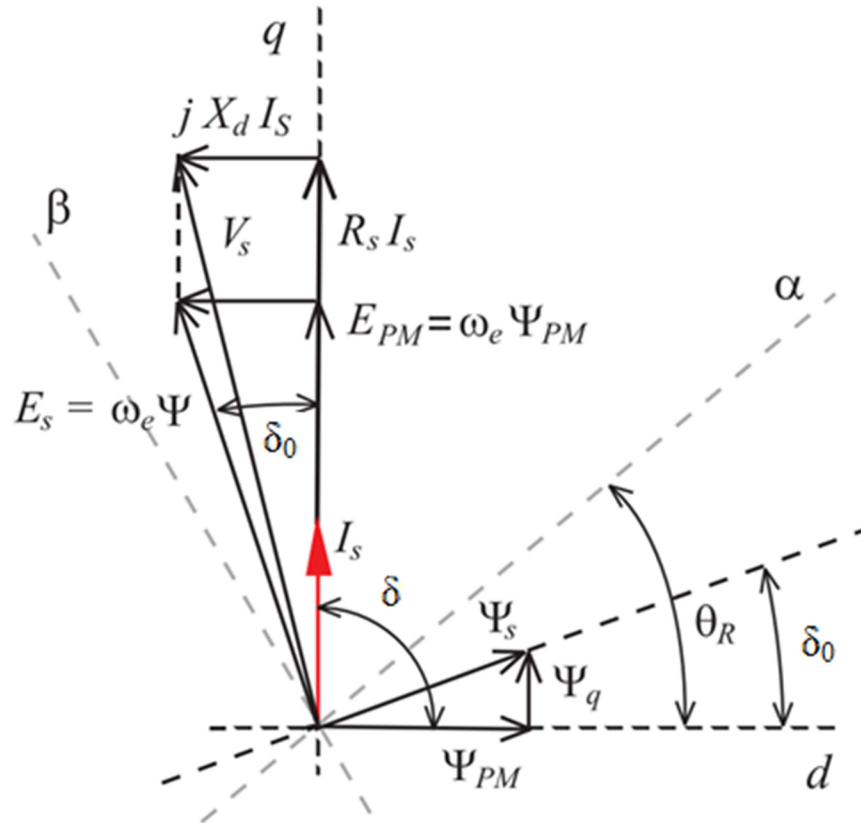
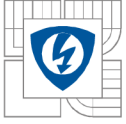


Fig 3.: Phasor diagram of vector controlled PM motor for maximum torque per stator current.[12]

In the load simulation these basic conditions are considered:

- The rated speed n :

$$n = \frac{60 \cdot f}{p} \quad (2.8)$$

- Applied voltage E_0 :

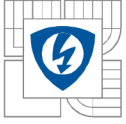
$$E_0 = \sqrt{2} \cdot V * \sin(2\pi \cdot f \cdot \text{time} + \left(\frac{\delta_0 \cdot \pi}{180}\right)) \quad (2.9)$$

Where is V is the RMS value of phase voltage, f is the frequency, δ_0 load angle:

In load simulation vector controlling of the machine is not considered, this may have a result in lower efficiency.

2.2.6 The traditional electrical machine design process

The traditional electrical machine design process is an iterative process. An assumption of machine efficiency eff_a and power factor pf_a has to be made and the machine rating S_{eff} in VA is calculated by equation (2.10):



$$S_{eff} = \frac{P_{out}}{eff_a * pf_a} \quad (2.10)$$

Where P_{out} is the specified machine rated output power. After the value for S_{eff} calculated, values for \bar{B} , ac and λ are selected to calculate D and L according to the sizing equation (2.1). Next, with the given rated voltage and current density, the number of coil turns and wire diameter of stator winding coils are determined for a given winding layout. At the same time, tooth width and core thickness are calculated with the selection of the flux density in the teeth and the core. The machine's outer diameter is then calculated from the slot area needed for the winding and the areas of the teeth and core. Rotor designs are also carried out with certain traditional rules, which can be found in the literature. After one complete trial design is produced, the performance of this trial design is calculated and verified against initially selected design parameters (primarily \bar{B} , ac , and J_s) and an assumption of efficiency and power factor. . [1] [2]

If any of these parameters does not agree with initially assumed values, modifications are made to either design parameters or assumptions and the design process is repeated. This process is repeated as many times as needed until agreement is reached. Even if such agreement is achieved, there are also various performance requirements to meet, such as specified maximum winding temperature, minimum power factor, and maximum weight. For line start induction machines, there are also requirements about starting current and starting torque. If one of such design requirements is not met, the designer has to modify the selection of certain design parameters and start the design process over with even more iterations. What make this traditional design process more time-consuming are the inherently complicated interrelations between different components of the machine. No direct relation exists between design parameters and machine performance so as to inform the designer about how to change design parameters to improve the design at the next iteration. Moreover, the inherent trade-offs between different machine performances indexes make it often impossible to improve one performance index without degrading another. For example, to increase machine efficiency, thicker wires can be used but this choice increases the weight and cost of the machine at the same time. In the traditional design, it is totally depend on the designer's personal experience and skill to find good designs through this iterative and heuristic process. Not only tedious and inefficient, this experienced-based design process cannot guarantee optimal machine performance with respect to its design specifications and operating environment, and this is a disadvantage in today's increasing application and performance requirement and competitive market of electrical machines.[1]

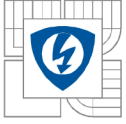
2.2.7 Analytical model for the optimization

Analytical model with some simplifications is used in optimization processes. The machine is assumed to operate under linear magnetic conditions, infinite permeability, and only the first harmonic is considered. This model is described in equations (2.11), (2.12), (2.13), and (2.14).[7]

The maximum electromagnetic power expression is:

$$P_{em} = 3 \cdot E_{RMS} \cdot I_{RMS} \quad (2.11)$$

Introducing a fill factor noted k_r and the current density per slot, noted as J_{RMS} , the load current can be written as follows in equation (2.12):



$$I_{RMS} = SFn \cdot J_{RMS} \cdot \frac{W_s \cdot SD}{Tph} \quad (2.12)$$

The EMF at no-load becomes [11]:

$$E_{RMS} = 2 \cdot \pi \cdot f \cdot (N_{spp} \cdot Tph) \cdot L_{rotor} \cdot (Rad1 + Gap) \cdot B_{fm} \quad (2.13)$$

Where B_{fm} is the first harmonic magnitude of the air gap flux density, it is given by equation:

$$B_{fm} = \frac{4}{\pi} \cdot \left(\frac{B_r}{1 + \frac{Gap}{LM}} \right) \cdot \sin\left(\frac{p \cdot BetaM}{2}\right) \quad (2.14)$$

In equations (2.12), (2.13) and (2.14) N_{spp} and Tph are respectively the number of slots/pole/phase and the number of conductor per slot.

Parameters $Rad1, Gap, BetaM, LM, L_{rotor}, SD, W_s, SFn$ are shown in, Table 3.2, Table 3.3, Table 3.4.

3 Description of significant parameters of machine

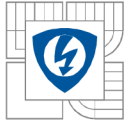
For simulation and optimization in this work, the slot per poles combination was defined as 12 /8 respectively. This work deals with simulation of PM machine by finite element method, using Ansoft Maxwell software. The results from simulations are compared with results of a parametric model, from SPEED Laboratory software. Results from both simulations methods are shown in figures and also compared between themselves.

3.1 Basic geometry and parameters of simulated machine

Machine parameters are described in this chapter. Parameters of the machine are divided in four main parts, the first of these shown the geometry of stator. In an-other subheads, parameters of rotor, stator windings and permanent magnets are described. In particular tables and figures the main parameters are shown. The other parameters are kept fixed, based on the original machine or derived, based on the AUTODESK software.

For a proper understanding of the analysed machine, the basic sizing should start with the equation (2.1)Substituting the basic geometry D, L , magnetic loading B and electric loading ac in to the equation (2.1), the motor rating should be calculated as follows:

$$S = 11 \cdot 0,866 \cdot 1,4 \cdot 49 \cdot \left(\frac{238}{1000}\right)^2 \cdot \frac{130}{1000} \cdot 3000 = 14394 W \quad (3.1)$$



In next step, the size of the aspect ratio λ from (2.2) should be calculated as follows:

$$\lambda = \frac{130}{(\pi \cdot 238)/4} = 0,695 \quad (3.2)$$

With this parameter, the winding induced EMF can be controlled and increased itself with less coil length.

The geometry of analysed machine is shown in Fig 4.

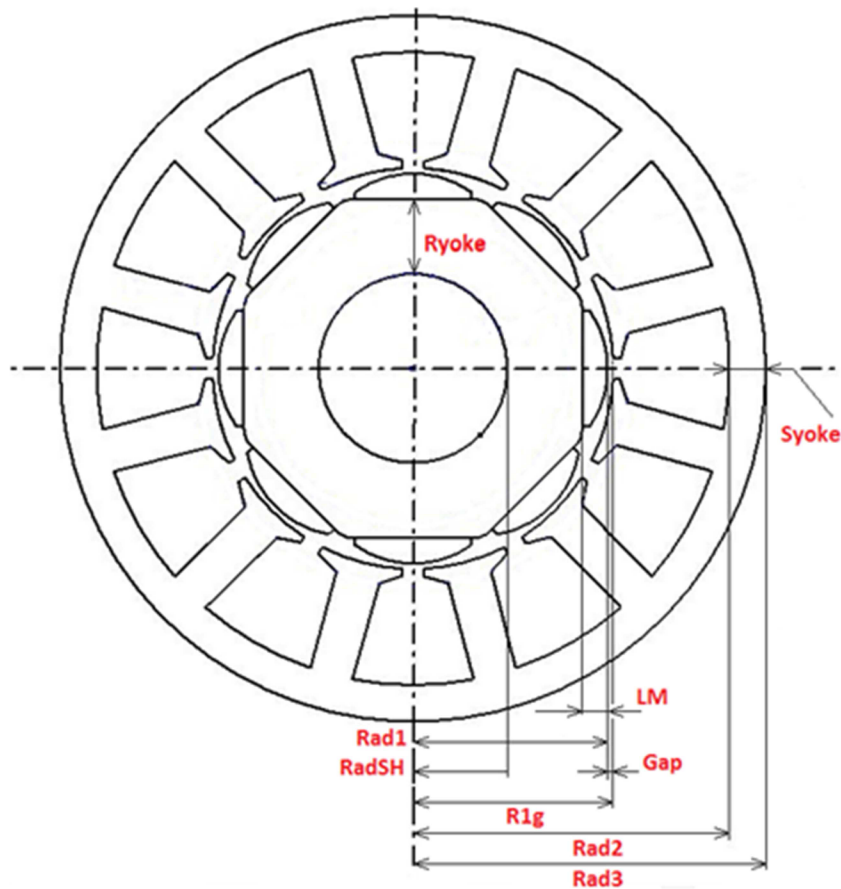
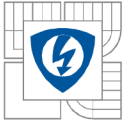


Fig 4.: Machine geometry [19]



3.2 Description of the basic stator parameters

Basic stator parameters and the slot geometry are shown in this paragraph. Slot geometry is shown on Fig 5. The Table 3.1 describes the basic dimensional parameters of the stator.

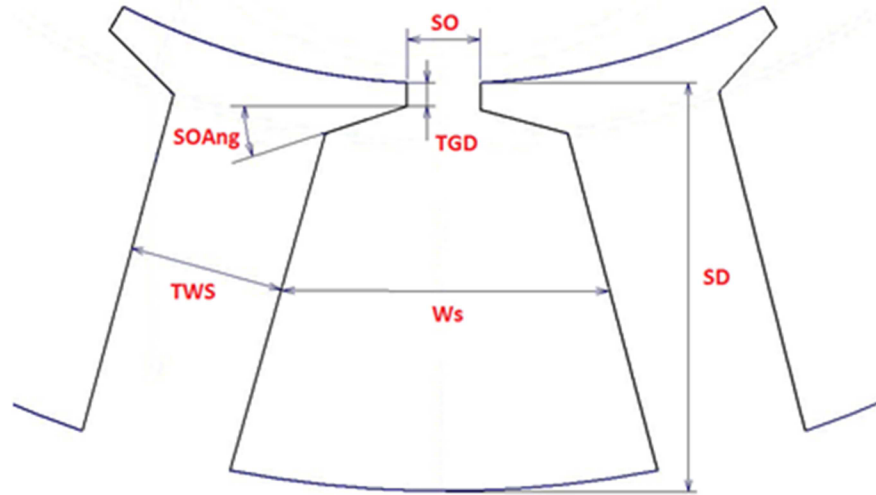
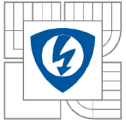


Fig 5.: Stator slot geometry [19]

Table 3.1: Basic stator parameters

PARAMETER NAME	LABEL	SIZE	UNIT	INDICATED IN:
Slot Opening	SO	4	[mm]	Fig 5
Tooth edge length in vertical axis	TGD	3	[mm]	Fig 5
Tooth width	TWS	21	[mm]	Fig 5
Slot depth	SD	37	[mm]	Fig 5
Slot opening angle	SOAng	20	[°]	Fig 5
Radial thickness of the stator yoke	Syoke	11,499	[mm]	Fig 4
Air-gap length	Gap	0,7	[mm]	Fig 4
Radius to the stator slot bottom	Rad2	107,501	[mm]	Fig 4
Largest radius in the motor cross-section	Rad3	119	[mm]	Fig 4
Medium slot width	W_s	25,6	[mm]	Fig 5
Length of stator	Lstator	139,548	[mm]	-



3.3 Description of the basic rotor parameters

In the Table 3.2 the basic dimensions of the rotor are described. For the simulations, the non-magnetic shaft was considered. Rotor geometry is shown in Fig 4.

Table 3.2: Basic rotor parameters

NAME	LABEL	SIZE	UNIT	INDICATED IN:
Thickness of the rotor yoke	Ryoke	22,9901	[mm]	Fig 4
Shaft radius	RadSH	42	[mm]	Fig 4, Fig 6
Rotor surface radius	Rad1	69,801	[mm]	Fig 4, Fig 6
Length of rotor	Lrotor	130	[mm]	-

The material used for the rotor is same as in the stator, the BH curve of M19_24 steel is shown in Fig 40(Enclosure A1).

3.4 Description of the basic magnet parameters

Very important for the proper function of the machine are permanent magnets. The dimensions of one pole are shown in Fig 6. The poles are mounted on outer surface of the rotor body. Distribution of the magnets is shown in Fig 4. In the Table 3.3 is description of the basic dimensional parameters of one pole.

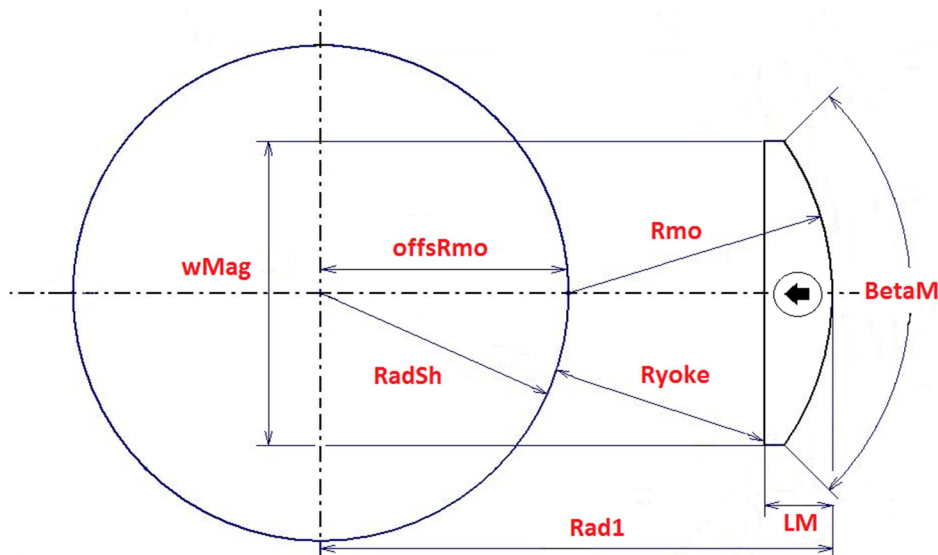


Fig 6.: Magnet parameters [19]

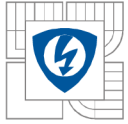


Table 3.3: Basic magnet parameters

NAME	LABEL	SIZE	UNIT	INDICATED IN:
Length of magnet	LM	8,848	[mm]	Fig 6
Pole arc	BetaM	160	[°e]	Fig 6
Width across one magnet	wMag	45,3473	[mm]	Fig 6
Circular arc radius of outer face of the magnet	Rmo	38	[mm]	Fig 6
Offset of arc radius Rmo	offsRmo	31,801	[mm]	Fig 6

Two different magnet materials for simulations are used. For the first design of the machine, the material Neodymium-iron-boron (NdFeb) of magnets is used. For the purpose of optimizing the material is exchanged for Samarium-Cobalt (SmCo). Properties of both used materials are shown in Enclosure B1 and C1.

3.5 Description of the basic winding parameters

The last of the main parameters important for the function of the machine are parameters of the stator winding. The distribution of all three phases in slots is shown in Fig 7. This distribution of the windings is called whole-coiled. Description of main windings parameters is in Table 3.4. How the simulation software works with these parameters is important to know. The difference between these parameters is as follows. The number of conductors per slot is the half of the value of turns.

Table 3.4: Basic winding parameters

NAME	LABEL	SIZE	UNIT	INDICATED IN:
Winding Layers	Layers	2	[-]	-
Winding Type		Whole coiled		-
Parallel Branches	PPath/2	4	[-]	-
Conductors per Slot	Tph	52	[-]	-
Coil Pitch	Offset	1	[-]	-
Number of Strands	NSH	10	[-]	-
Wire Size	WireDia	0,6077	[mm]	-
Slot liner	Liner	0,4	[mm]	-
Layer insulation	InsThick	0,0313	[mm]	-
Limited fill factor	SFn	0,568	[-]	-

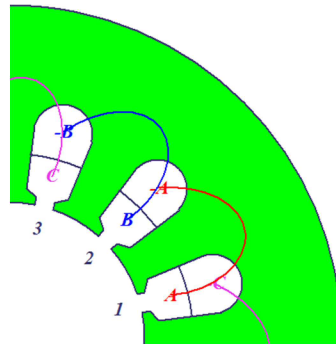
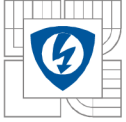


Fig 7.: Winding distribution in the slots

3.6 Created Parametric model

For purposes of this master thesis a parametric model of the machine was created. Each geometric dimension is represented by its parameter, and the parameter value can be changed at any time, for the purposes of the simulation. The example of change of a parameter is shown in Table 3.5. The geometrical dimensions and other parameters of the machine are described in Chapter 3.

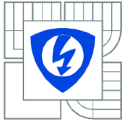
The advantage of the created model is the ability to quickly change the selected machine dimensions and thus effectively find the ideal dimensions of the machine. Parametric model will be further used for optimization in a last chapter of this thesis.

Table 3.5: Example of changing the magnet geometry by changing the parameter offsRmo

OffseRmo = 0 mm	OffsetRmo = 31,801 mm

4 Selected simulations performed on parametric model

In this chapter results of simulations and calculations are evaluated. Simulations for different densities of finite element mesh were performed. Number of elements in finite element mesh affects the accuracy of the results of each simulation. In this work 3 types of mesh are used. Comparison of the number of elements for 3 selected meshes is presented in Table 4.1. The differences between meshes are shown in Fig 8, Fig 9, and Fig 10. Choosing the right mesh affects the simulation results. Number of elements in the network increases the accuracy of the simulation, but not always. If we use a large number of elements, that will increase simulation times. The aim of simulations with different networks is to determine the zone where the simulation accuracy is close to 5% and does not take so



much time. Moreover, it is not necessary to have a fine mesh throughout the model, but focus on the most important part of each simulation. Simulations at two different temperatures, namely 25 ° C and 125 ° C are performed. For the purpose of optimization, the material of permanent magnets is changed. Neodymium-Iron-Boron (NdFeB) magnets are used for original design. For the new design of machine the Samarium-Cobalt (SmCo) magnets are used. The material properties of permanent magnets for both temperatures 25°C and 125°C are set differently. Permanent magnets materials properties are described in enclosure B1 and C1. Demagnetization analysis are described in chapter 4.8.

Table 4.1: Number of elements in selected meshes

NAME OF THE MESH TYPE	NUMBER OF ELEMENTS	UNIT	INDICATED IN
Mesh	18962	[-]	Fig 8
Mesh3	158412	[-]	Fig 9
Mesh5	393775	[-]	Fig 10

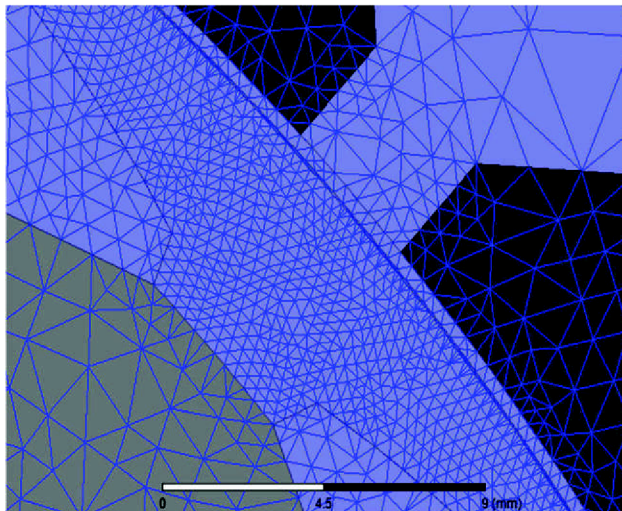


Fig 8.: Plotted mesh in the geometry of machine.

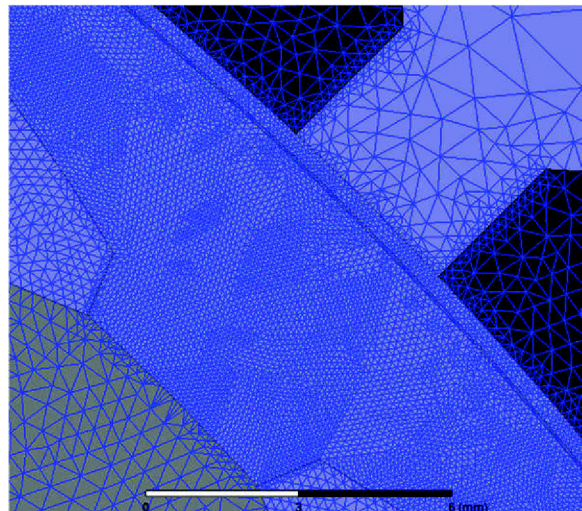


Fig 9.: Plotted mesh3 in the geometry of machine.

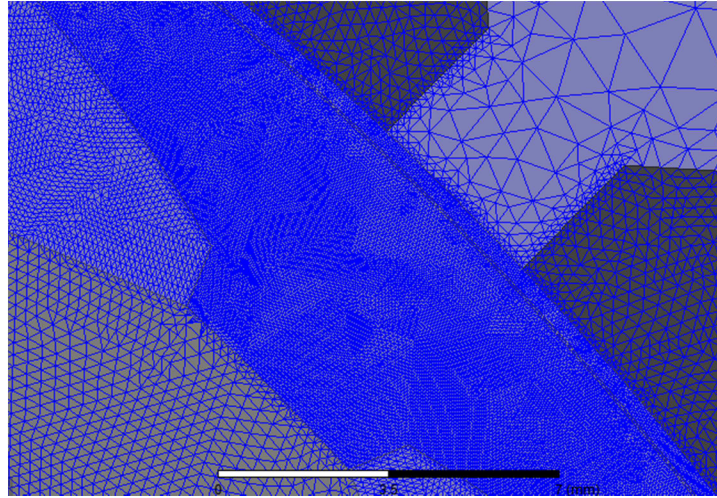
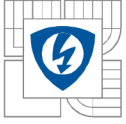


Fig 10.: Plotted mesh5 in the geometry of machine.

4.1 Induced voltage

The value of induced voltage of analysed machine is obtained from no-load simulation. For calculation basic equation (2.13) is used, where E_{RMS} , is the effective value of induced voltage of one phase. [1],

$$E_{RMS} = 2 \cdot \pi \cdot f \cdot (N_{spp} \cdot Tph) \cdot L_{rotor} \cdot (Rad1 + Gap) \cdot B_{fm} \quad (4.1)$$

Where B_{fm} is the first harmonic magnitude of the air-gap flux density created by magnets.

In equations (4.1) N_{spp} and Tph are the number of slots/pole/phase and the number of conductor per slot respectively. Parameters $Rad1$, Gap , L_{rotor} are shown in Table 3.2

The value of induced voltage for 3000 rpm:

$$E_{RMS} = 2 \cdot \pi \cdot 200 \cdot (0,5 \cdot 52) \cdot 0,13 \cdot 0,0705 \cdot 0,577 \cdot 1,1 = 190,1V \quad (4.2)$$

Simulation conditions are observed in the simulation of induced voltage as follows. Model is simulated by using transient setup. Input currents to windings are set as a zero current. The speed of a rotor is set to 3000 rpms in motion setup. Simulation runs only on one quarter of the machine. Induced voltage curves were determined for the selected mesh (Fig 8) and mesh5 (Fig 10).

The waveforms of immediate value of induced phase voltage from Maxwell no-load simulation on parametric model depending on the rotor position for two different meshes and simulation temperatures are shown in following figures Fig 11, Fig 12, Fig 13 and Fig 14.

The differences between the induced voltage waveforms for two different temperatures are shown in Fig 11, Fig 12 and Fig 13. All waveforms of the induced voltage are shown as Line-to-Line value.

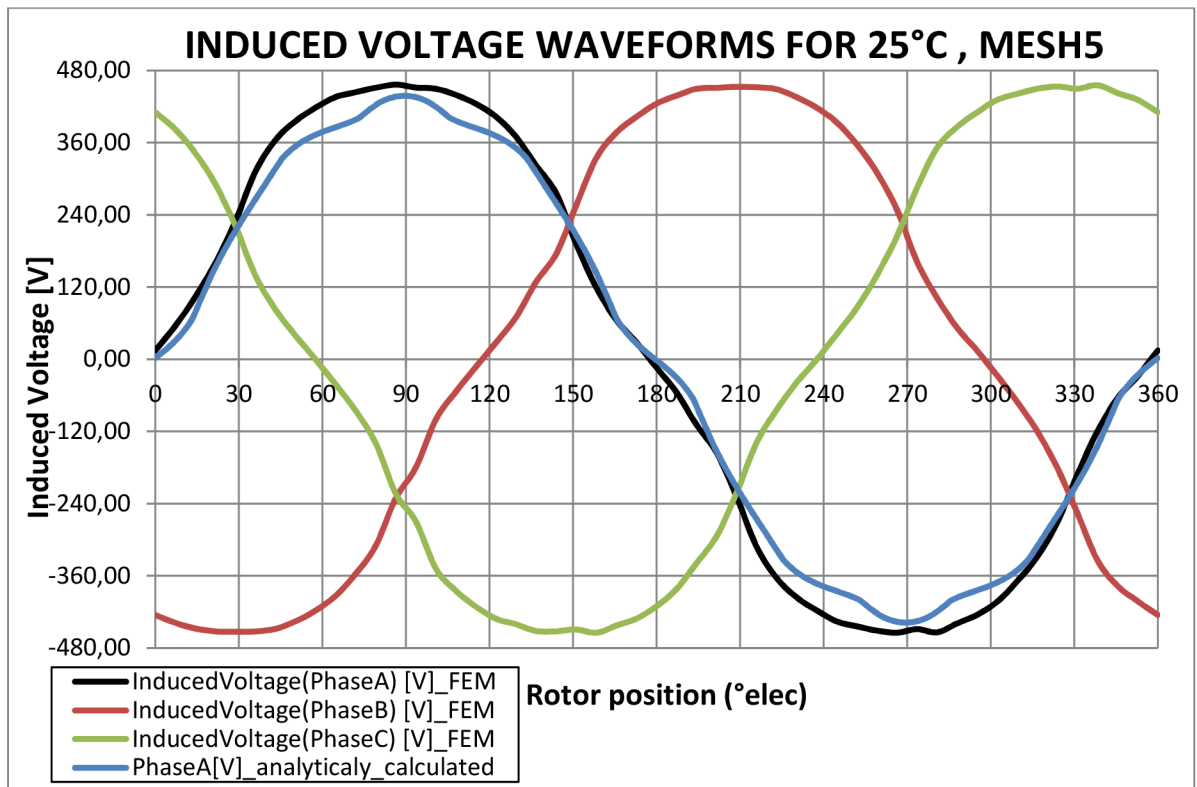
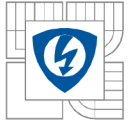


Fig 11.: Induced voltage for simulation temperature 25°C, NdFeB magnets.

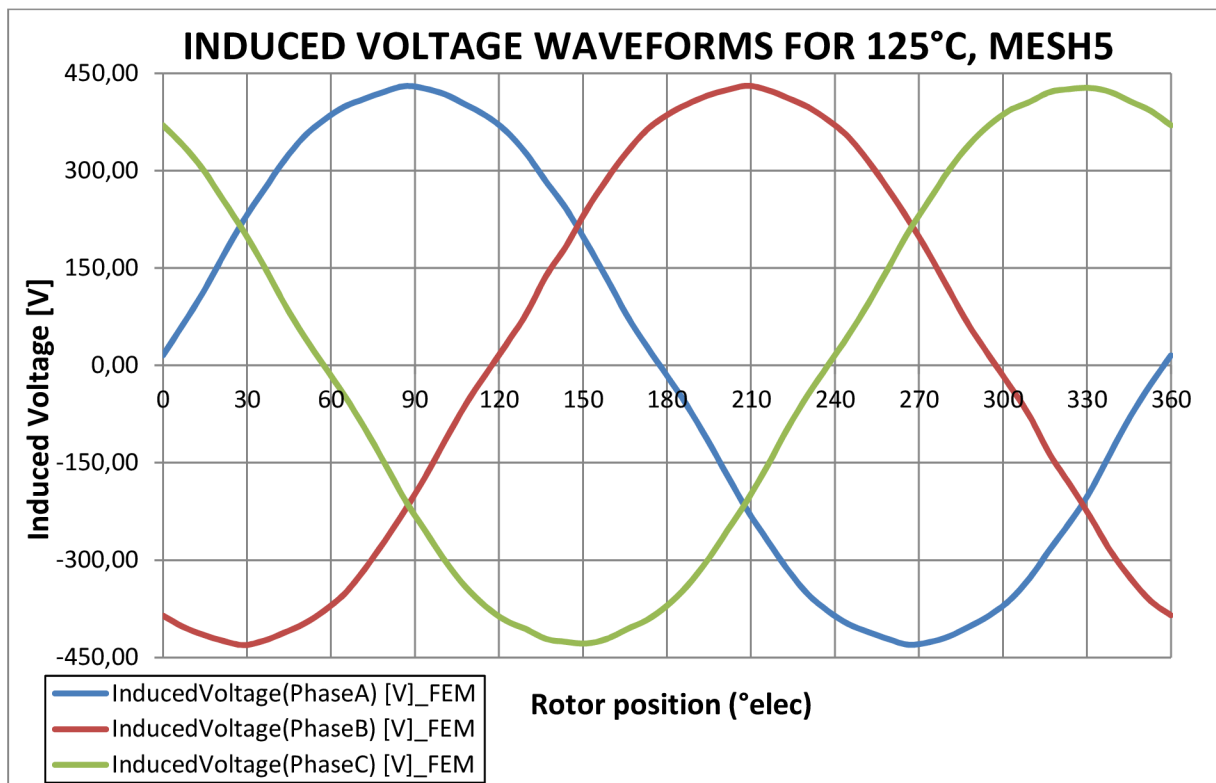


Fig 12.: Induced voltage for simulation temperature 125°C, NdFeB magnets.

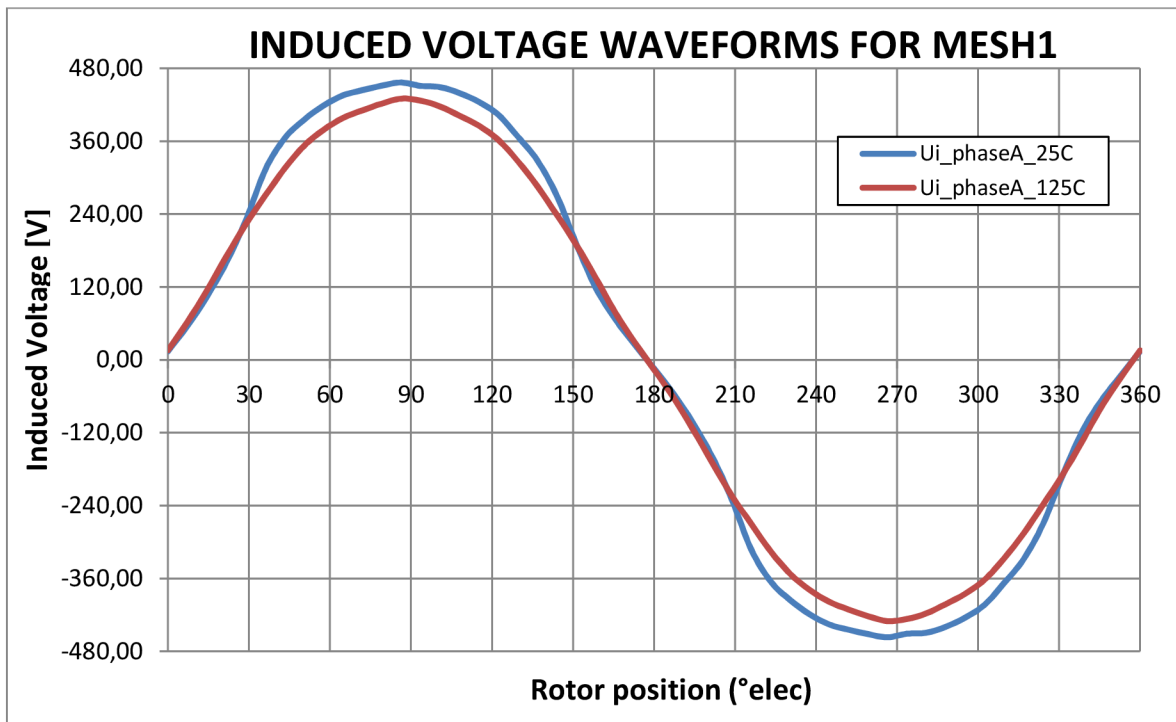
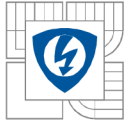


Fig 13.: Induced voltage waveforms simulated at different temperatures, NdFeB magnets.

For the evaluation, the waveforms of induced voltage from Maxwell and Speed were compared with analytical results. The differences between all applied methods of the calculation are shown in Fig 14. The value of induced phase voltage is calculated in equation (4.2).

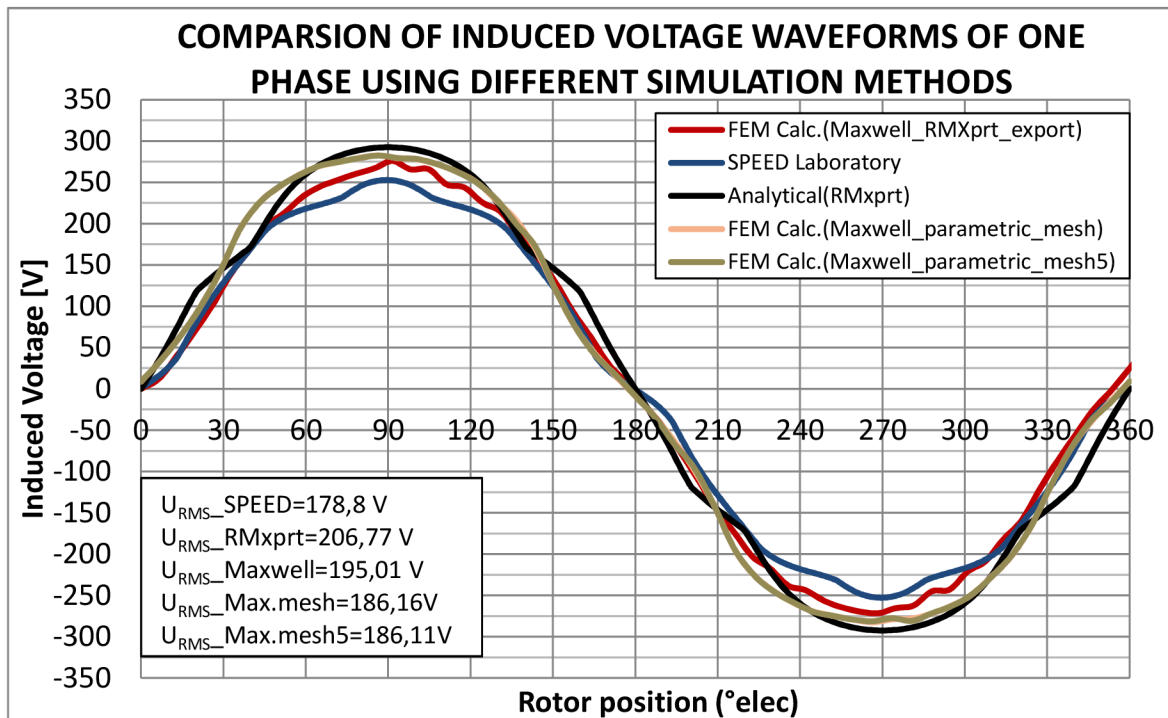
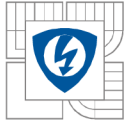


Fig 14.: Induced voltage waveforms from different simulation software, NdFeB magnets



The waveform of immediate value of one induced phase voltage from SPEED Laboratory is shown in Fig 14. Differences between waveforms from Maxwell and from SPEED are given by different access to calculate. For the basic calculation of induced voltage, the SPEED software uses the mathematic model and MAXWELL uses the finite element method. In SPEED, the FEA calculation has to be done and the analytical model has to be adjusted on the FEA model by X-Factors coefficients X-Factor match is not the part of this work.

Same simulation for describe the waveforms of induced voltage with new material of permanent magnets is simulated. In parametric model the new magnet material is defined. Properties of new material for the simulation temperature are set to parametric model. Results of simulation with new permanent magnet material at 125°C are shown in Fig 15.

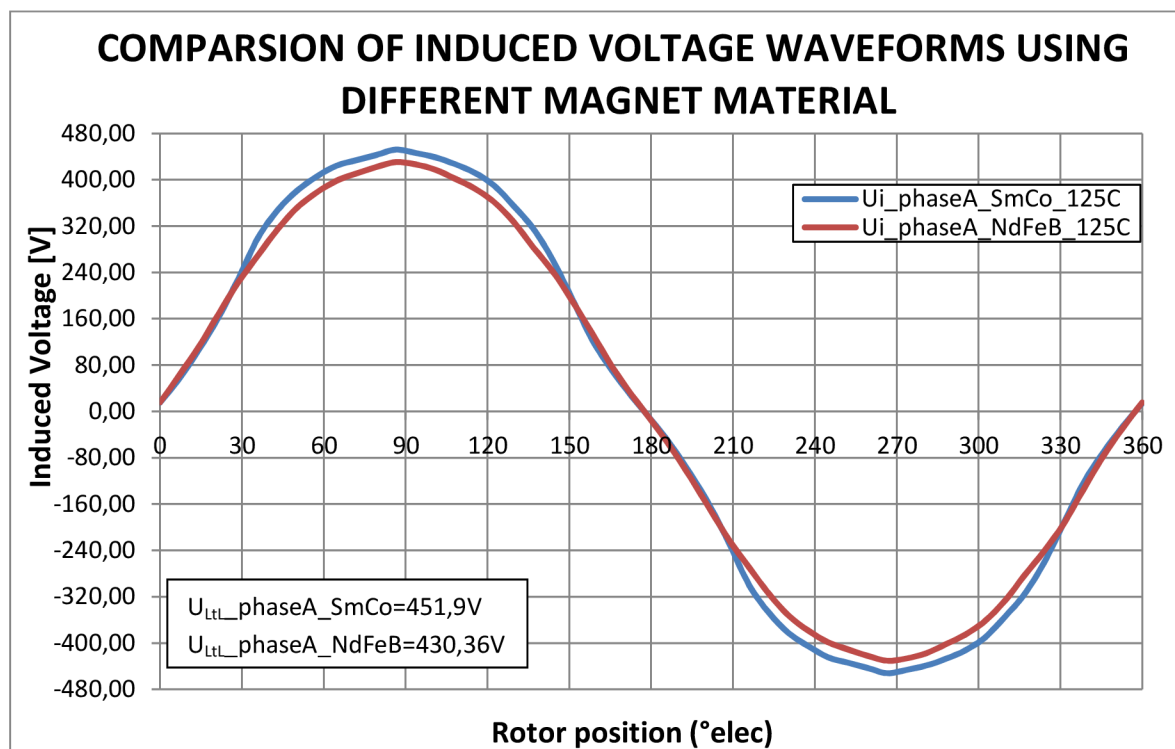
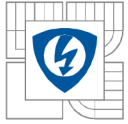


Fig 15.: Comparison of induced voltage waveforms using different permanent magnets material

In Fig 15 the differences between line to line induced voltage waveforms with two different magnet materials are shown. The induced voltage waveform from simulation with NdFeB magnets is affected by changes in material properties due to temperature. Worse properties of NdFeB magnets at a temperature of 125°C are proved by these curves. Improved characteristics of the new SmCo magnet at this temperature are detected. Line to line value of induced voltage is increased by 21,5 V due to change of permanent magnets material.

4.2 Cogging torque

One of the main disadvantages of PM machines is the torque ripple. This ripple torque is parasitic, and can lead to mechanical vibration, acoustic noise, and problems in drive systems. Minimizing this ripple torque is of great importance in the design of a PM machine. One of the main contributors to this torque ripple is cogging torque, which is the interaction between the permanent magnets and the stator slots [11].



Simulation conditions in the simulation of cogging torque as follows are observed. Model is simulated by using of the transient setup. Zero currents to windings are set as the excitations. The rotor speed is set in degrees per second in motion setup. On the rotor body a parameter torque is set. On this parameter the curves of cogging torque are plotted and evaluated. Waveforms of cogging torque over one stator slot (30 mechanical degrees) are obtained. Simulation runs only on one quarter of the machine. Cogging torque values were determined for the selected mesh (Fig 8), mesh3 (Fig 9) and mesh5 (Fig 10).

The minimalizing of cogging torque is one of the tasks for the optimization. The aim of this study was to determine the waveforms of cogging torque. In Table 4.2 the values of individual cogging torque with different simulation conditions are compared. The waveforms of the cogging torque for different mesh types and temperatures depending on the angle of the rotor position are shown in Fig 16 and Fig 17.

Table 4.2: Cogging torque values at different simulation conditions for NdFeB magnets.

		samples per period[-]					
		30		60		100	
		Cogging torque[Nm]	Error[%]	Cogging torque[Nm]	Error[%]	Cogging torque[Nm]	Error[%]
25°C	mesh	3,675	3,8722	3,687	4,2015	3,939	11,32
	mesh3	3,513	-0,7038	3,503	-0,9780	3,546	0,23
	mesh5	3,510	-0,7914	3,499	-1,1108	3,538	ref. val.
125°C	mesh5					1,140	

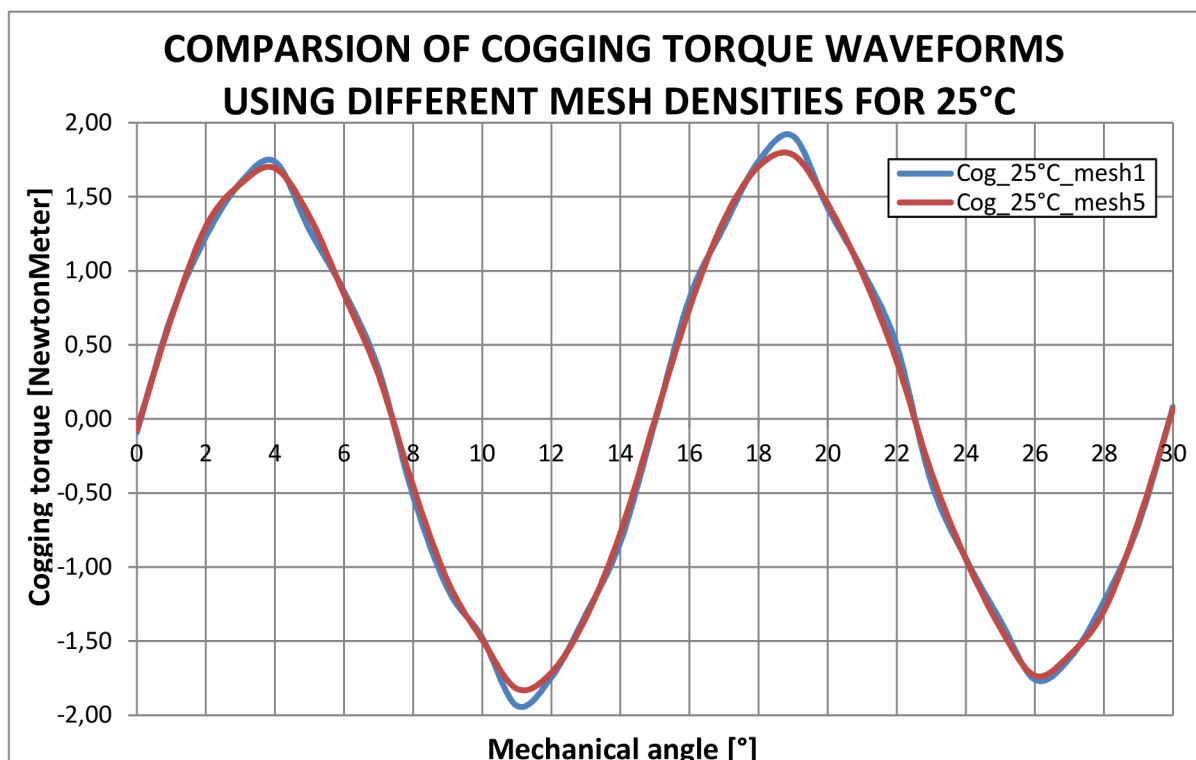


Fig 16.: Cogging torque waveforms at different mesh conditions, 25°C, NdFeB magnets.

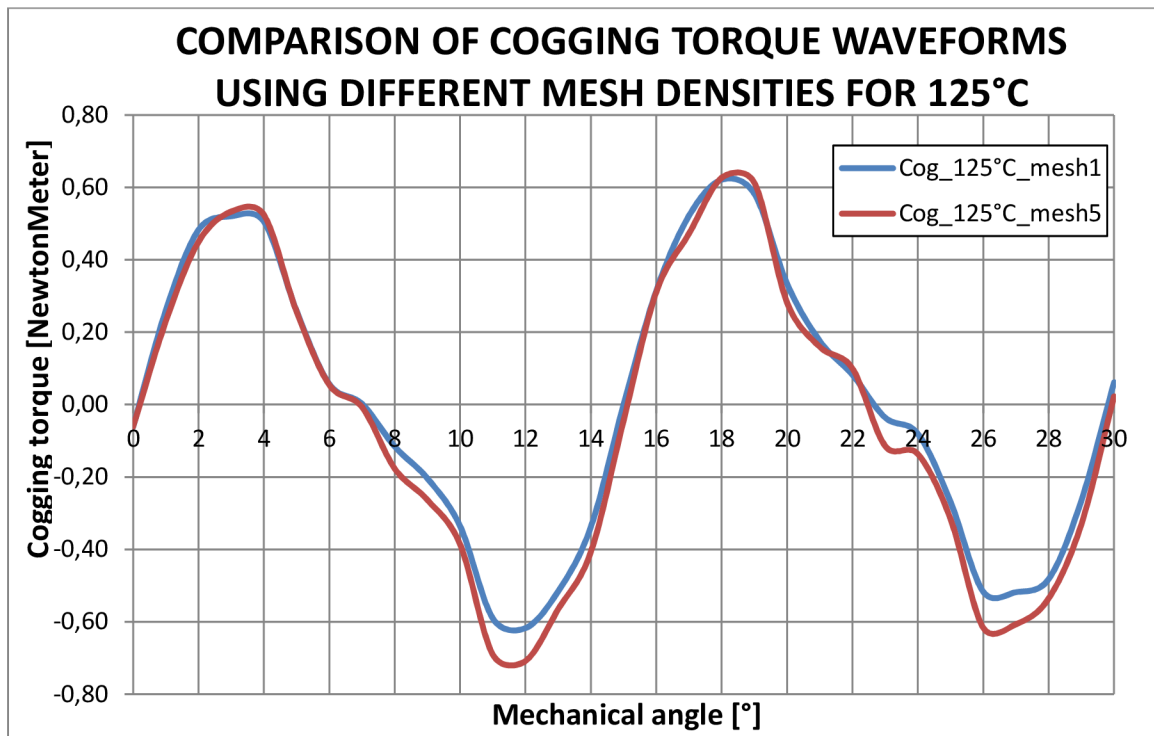
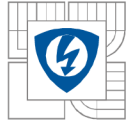


Fig 17.: Cogging torque waveforms at different mesh conditions, 125°C, NdFeB magnets.

The comparison of different cogging torque waveforms are shown in Fig 18. Waveforms of curves from various simulations are given by different temperatures. With the change of temperature occurs to change the properties of permanent magnets and thus change cogging torque waveform.

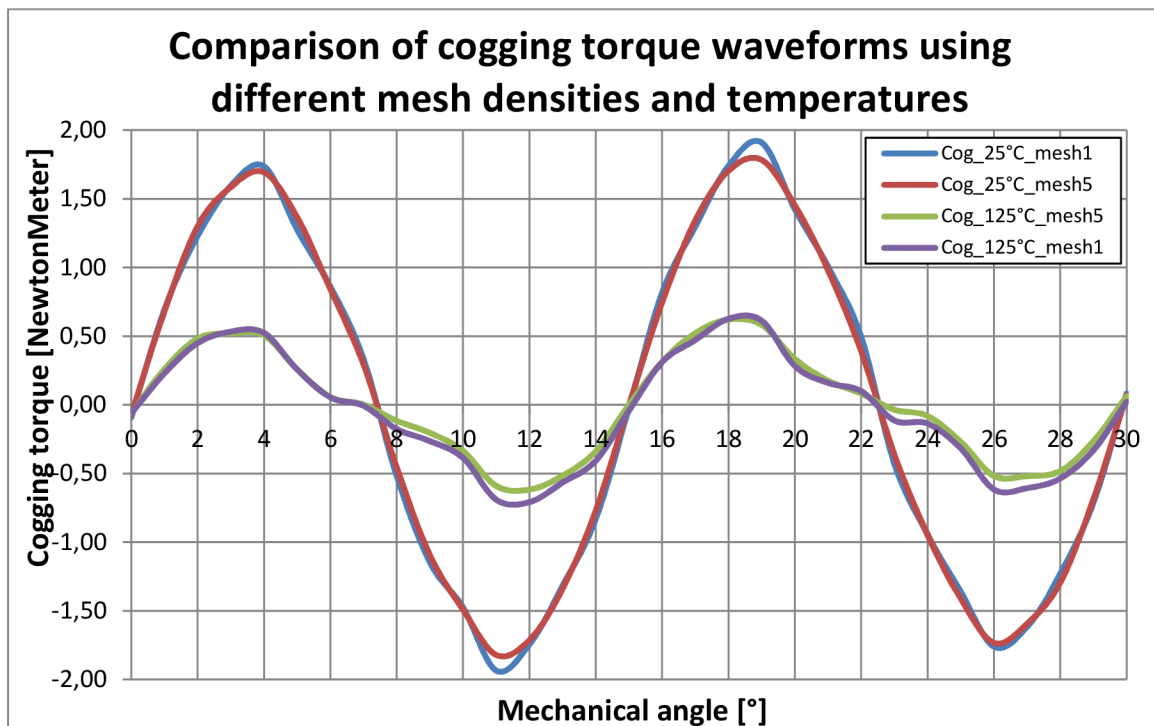
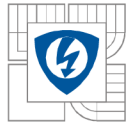


Fig 18.: Cogging torque waveforms in different simulation conditions, NdFeB magnets



Due to changes in permanent magnets material the new simulation of cogging torque at temperature 25°C is performed. Results from this simulation with new SmCo magnets are shown in Fig 19, as comparison with waveform of cogging torque simulated with NdFeB magnets.

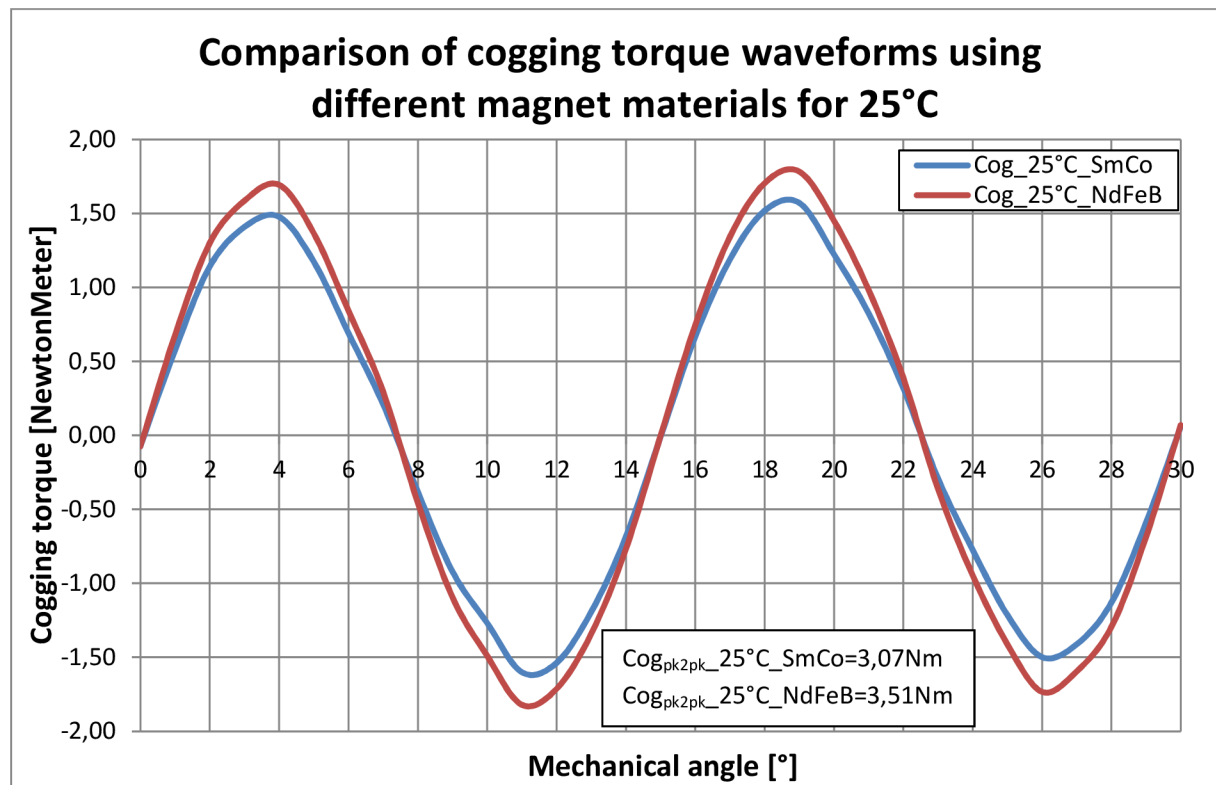


Fig 19.: Comparison of cogging torque waveforms using different permanent magnet material

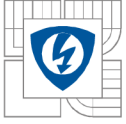
For evaluation peak to peak, values of cogging torque properties of the magnets at a given temperature are again important. NdFeB magnets have better properties in temperature 25°C. Value of cogging torque is more influenced by magnets with better performance. Worse properties at higher temperatures is big a disadvantage of NdFeB magnets. At higher temperatures the value of cogging torque with SmCo magnets is higher. The difference between values of both permanent magnets material is 0,44 Nm. Diminution of cogging torque value is one of the optimization issue in chapter 6.

4.3 Evaluation of the steady torque

For evaluation of steady torque two different simulations are used. Steady torque is evaluated from Maxwell simulation on model given by Rmxprt, in the first part of this chapter. Steady torque simulation is carried out at a temperature of 125°C. Simulation on Rmxprt's model from is simulated for condition when motor starts from stand still to rated speed. For Simulations on parametric model another approach is used. Simulation takes less time and the value of steady torque is more accurate. Steady torque waveforms for NdFeB and SmCo magnets are compared and evaluated.

4.3.1 Load simulation in Rmxprt

In load conditions simulation the nominal value of voltage is attached to the terminals. During the load simulation, the machine started from standstill, and accelerated to the rated speed n . Two options are available for load of the machine. In this simulation machine is loaded by torque angle δ . No load on the shaft is considered. The machine torque definition shows the equations (2.4), (2.5) and (2.6).



From load simulation, waveforms of machine torque and winding currents during the start of the machine are described.

The basic conditions in load simulation were these:

- The transient simulation was used. Time of the simulation was: $t = 120 \text{ ms}$
- The rotor speed n from equation (2.8) was set:

$$n = \frac{60 \cdot 200}{4} = 3000 \text{ rpm} \quad (4.3)$$

- Applied voltage E_0 was set according to the equation, for time $t_1 = 110 \text{ ms}$ (2.9).

$$E_0 = \sqrt{2} \cdot 230 \cdot \sin\left(2\pi \cdot 200 \cdot 0,11 + \left(\frac{11,04 \cdot \pi}{180}\right)\right) = 215 \text{ V} \quad (4.4)$$

4.3.2 Load torque characteristic

The values of torque at load simulation are calculated by 3 different methods. Analytically from RMxprt module, from mathematical model by SPEED, and from finite elements method by Maxwell are these three methods. The steady value of torque is calculated by equations (2.4), (2.5) and (2.6). Example of calculation is shown in equations (4.6), (4.7) and (4.8).

$$T_e = T_{e1} \sin \delta + T_{e2} \sin 2\delta \quad (4.5)$$

Where is:

$$T_{e1} = \frac{3 \cdot 4 \cdot 230 \cdot 215}{2\pi \cdot 200 \cdot 3,8} = 123,68 \text{ Nm} \quad (4.6)$$

Values of reactance X_d and X_q are calculated from inductances evaluated in chapter 4.7:

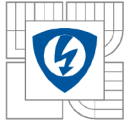
$$X_d = 3,8 \ \Omega \quad X_q = 46,87 \ \Omega$$

And the reluctance torque T_{e2} is calculated from these values:

$$T_{e2} = \frac{3 \cdot 4 \cdot 215^2}{4\pi \cdot 200} \left(\frac{46,87 - 3,8}{3,8 \cdot 46,87}\right) = 53,37 \text{ Nm} \quad (4.7)$$

With these two components of load torque is calculated the value of torque for angle $\delta = 12^\circ$. the value of torque angle was chosen deliberately because, the value of load angle is $\delta_0 = 11,04^\circ$. This issue is shown in Fig 1 . The calculated torque from the equations is:

$$T_e = 123,68 \cdot \sin\left(\frac{12 \cdot \pi}{180}\right) + 53,37 \cdot \sin\left(2 \cdot \left(\frac{12 \cdot \pi}{180}\right)\right) = 47,8 \text{ Nm} \quad (4.8)$$



The Fig 20 shows the torque characteristic from load simulation in Maxwell, on the model exported from Rmxprt. The waveform of torque during the start of the machine from standstill position is shown in the figure. In Fig 20 the detail oscillations of the torque around average value is also shown. These oscillations are given by the ripple and cogging torque. This torques can also be eliminated by the optimization of the machine.

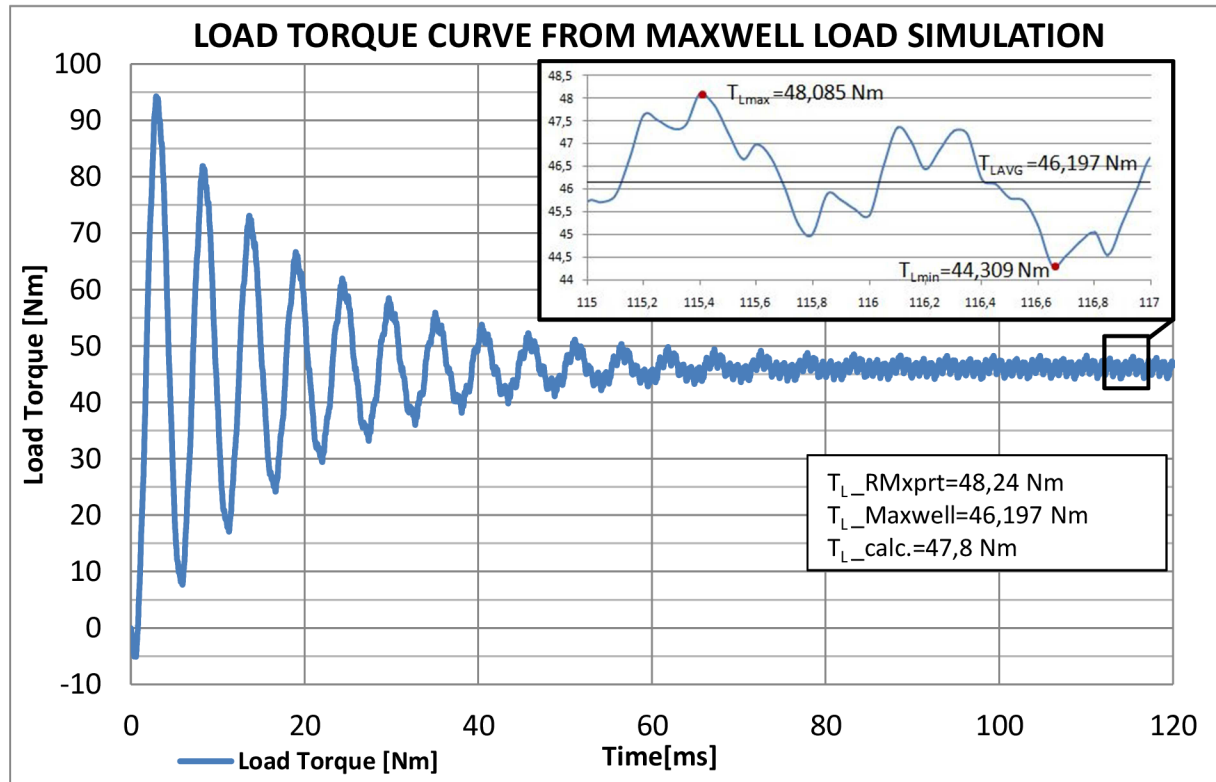
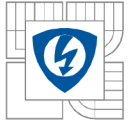


Fig 20.: The torque waveform from simulation on model given by Rmxprt, NdFeB magnets.

Comparison of the values obtained by different methods is also shown in Fig 20. The differences between values are small but they are certainly influenced by the accuracy of the models and calculations.

4.3.3 Load torque winding currents waveforms

Waveforms of phase currents in each phase are corresponding to the torque characteristic. Stator windings task is to create the rotating magnetic field. The speed of this magnetic field is synchronous, calculated in equation (4.3). This stator magnetic field draw the rotor field into synchronism. The speeds of both magnetic fields are not the same in every time due to the swinging of the rotor. The swinging of the rotor is also shown in torque characteristic in Fig 20. The character of waveforms of phase currents in Fig 21 during the start-up are not the same as in the steady state, for this reason When the machine starting up from standstill state, the higher currents will flow through the windings, to obtain a large enough magnetic field. When the rotor speed starting to be high enough, currents waveforms are starting to being reduced and when the speed is on rated value n , the waveforms of windings currents is stabilized at the nominal value. The pulsations of the currents during the start-up are influenced by the synchronous speed of the machine. During the start-up, the synchronous speed was not achieved, because of the high shaft torque and also high values of the current.



The example of calculating of the RMS value of phase current is shown in equation (4.9):

$$I_{RMS} = 0,568 \cdot 2,5 \cdot \frac{25,6 \cdot 37}{52} = 25,8A \quad (4.9)$$

The waveforms of phase currents of analysed machine are shown in Fig 21. These values were given by the finite elements method simulation using Maxwell.

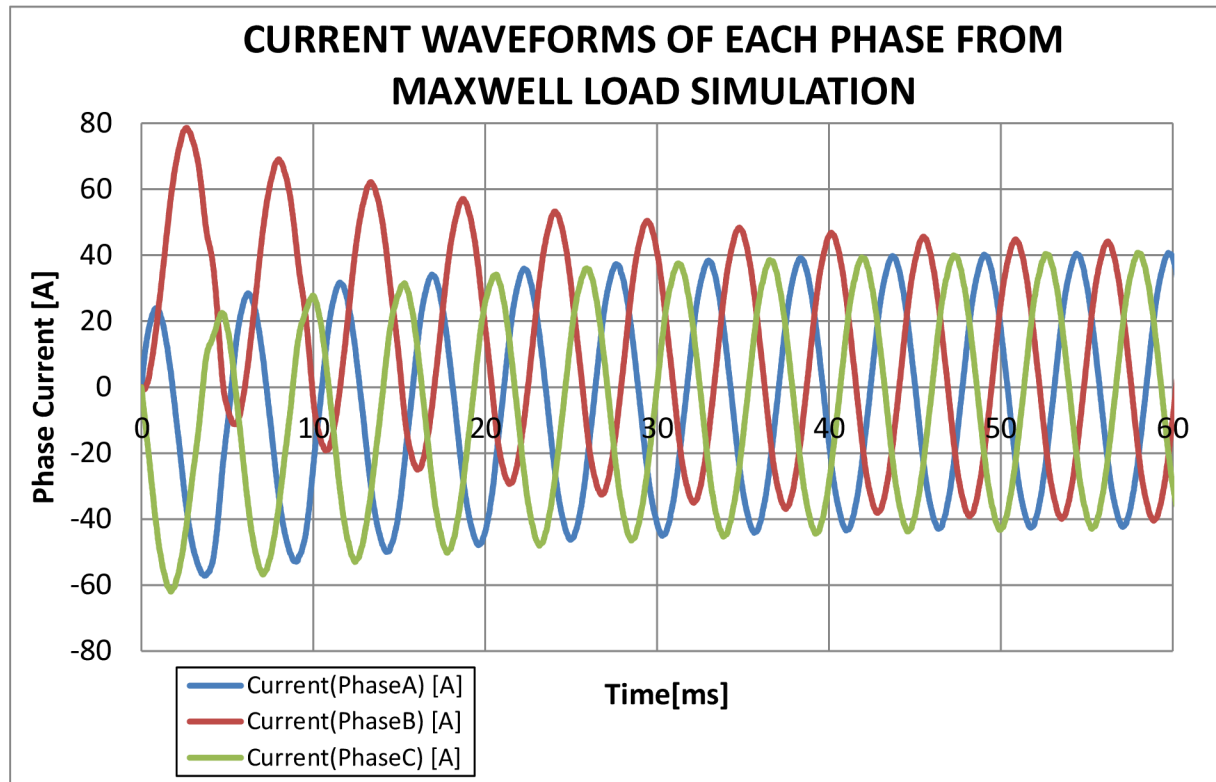


Fig 21.: Winding Currents

4.3.4 Steady torque simulated on parametric model

The correct parametric model is simulated for evaluation of steady torque waveforms for both used permanent magnet materials. The advantage of parametric model and its simulation is simulation time only 4 ms. Steady torque waveforms is shown in Fig 22. Values from simulation on parametric model are shown in Table 4.3.

Table 4.3: Values of steady torque from parametric model simulation for both PM material

Permanent magnets material	$M_e [Nm]$
NdFeB	41,9 Nm
SmCo	44,4 Nm

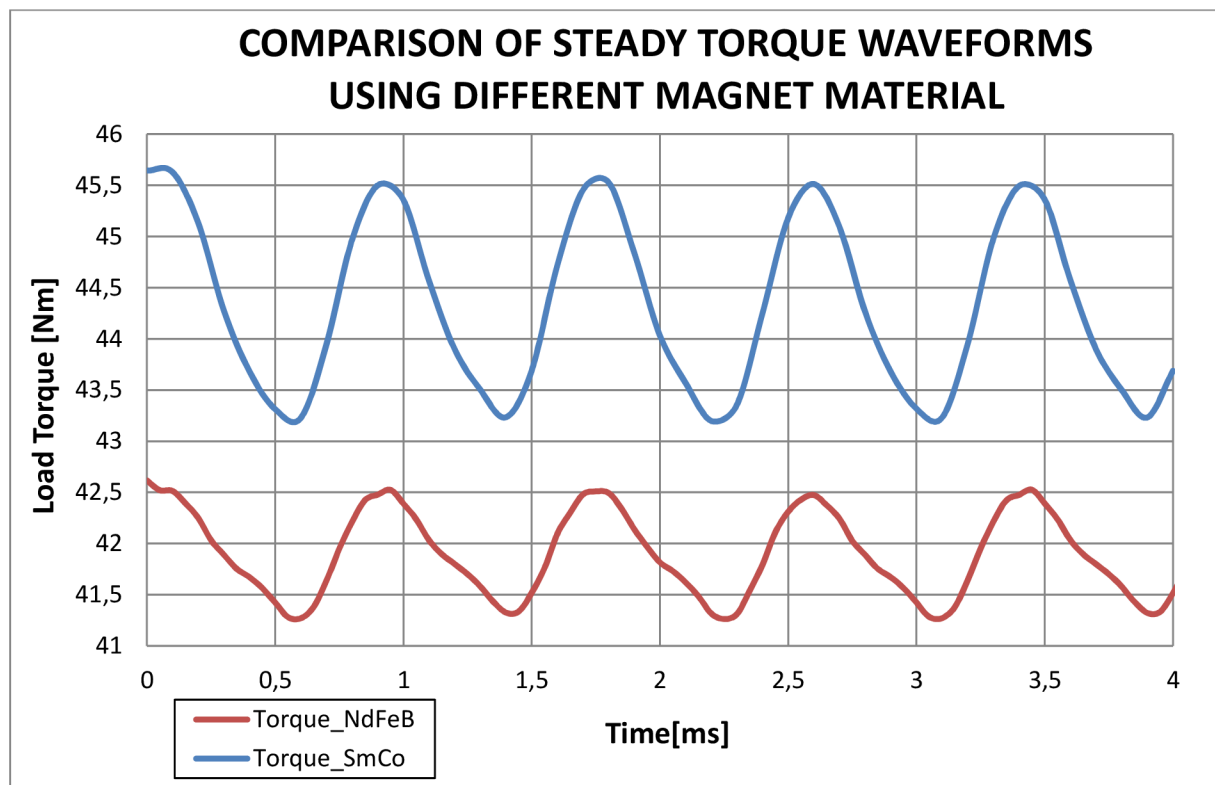


Fig 22.: Steady torque waveforms for two different permanent magnets material.

The differences between waveforms and values of steady torque are given by PM properties at temperature 125°C. Dimensions of PM are not changed for new material. From steady torque waveforms the values of steady torque are obtained. Values of steady torque with NdFeB magnets is 41,9 Nm, and value of steady torque with Smco magnets is 44,4 Nm.

As the induced voltage simulation at this temperature, better values with SmCo magnets are achieved. On the waveform of steady torque for SmCo magnets bigger value of cogging torque is shown. Minimization of cogging torque is one of the optimization issue described in chapter 6.

The differences between the values of the steady torque of the different types of simulation are also given by different approaches of each simulation tools. In parametric model simulation core and solid losses are considered. Geometry of Rmxprt model in certain parameters is different from parametric model geometry. Values given by simulation on parametric model are more accurate. Values of steady torque are not identified using vector control. The values of steady torque can be maximized with use of vector control.

4.4 Flux density distribution in machine geometry

To verify the accuracy of the simulated model of electrical machine is important the proper distribution of flux-density in the machine body. These distributions for both simulated conditions are shown in Fig 23 and Fig 24. The distribution of flux-density in one quarter of machine in no-load simulation is shown in Fig 23. Windings currents are set to zero and the shaft is rotating by moving torque on rated speed n in this simulation. On the detail view in Fig 23, the over saturation of the stator tooth corners due to the scattering fluxes is shown. This over saturation also influences the waveforms of flux-densities in the air gap.

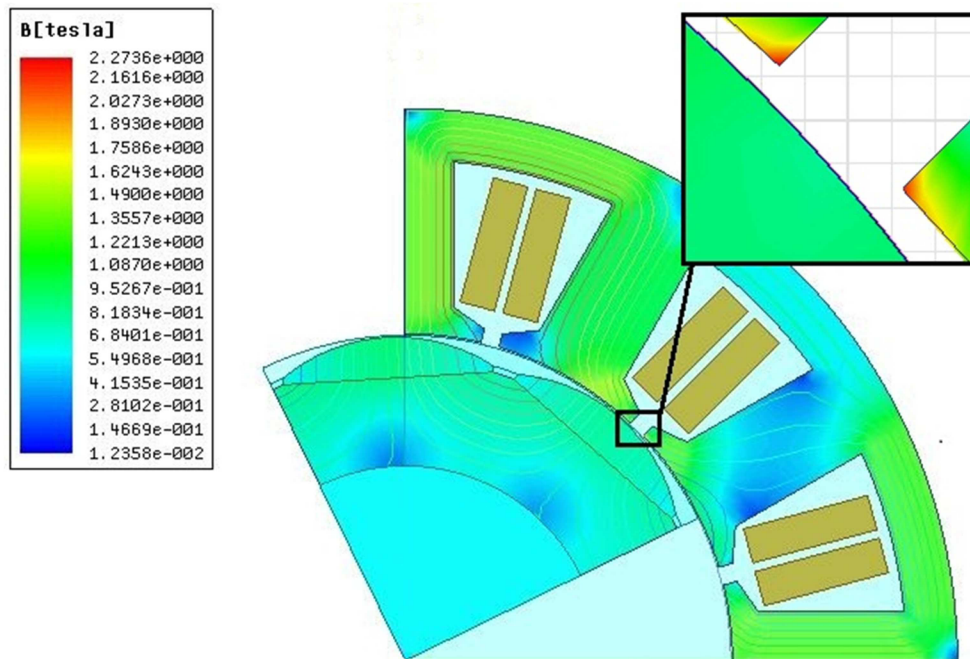
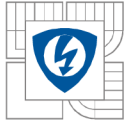


Fig 23.: Detail of saturation in teeth corners in no-load conditions

The Fig 24 shows the saturation of machine body in load condition. In load conditions simulation the nominal value of voltage is attached to the terminals. During the load simulation, the machine started from standstill, and accelerated to rated speed n . In the Fig 24 are shown places where the value of saturation is very small, these places could be replaced by air gap.

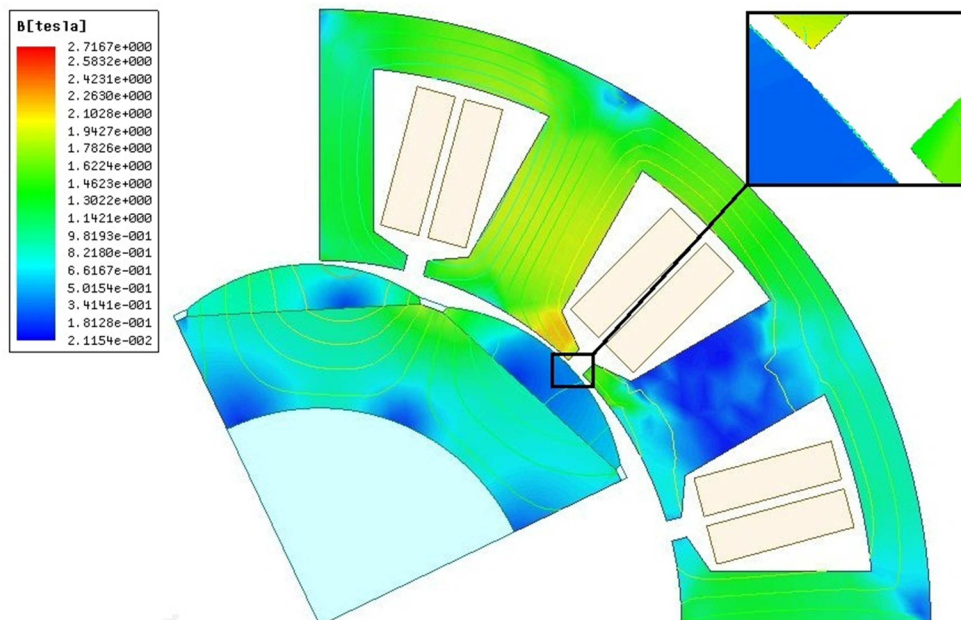
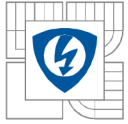


Fig 24.: Detail of saturation in teeth corners in load conditions

The load simulation does not show the over saturation in tooth corners because the machine is working in right operating conditions for which it was designed.



4.4.1 Radial flux density distribution in the air gap

The distribution of flux-density in the air gap is also important for a good function of the machine. The air gap flux-density is usually described by means of two basic components. The first of these components is the radial flux-density. The value of radial flux-density is calculated by equation (4.10):

$$B_{rad} = B_x \sin \theta + B_y \cos \theta \quad (4.10)$$

Example of calculation B_{rad} for the rotor position angle $\theta = 253^\circ$ is shown in equation (4.11), (4.6):

$$B_{rad} = 0,718 \cdot 0,819 + 0,494 \cdot 0,5737 = 0,871 \text{ T} \quad (4.11)$$

The Fig 25 shows the distribution of radial flux-density in the air gap. The figure shows two curves of B_{rad} calculated by Maxwell and by SPEED Laboratory. The curves are influenced by stator slot shape and the gaps between teeth of the stator. Differences between curves calculated by Maxwell and SPEED are given by different calculations methods. The curve from Maxwell simulation was several times recalculated, and also controlled by equation (4.10) in few points.

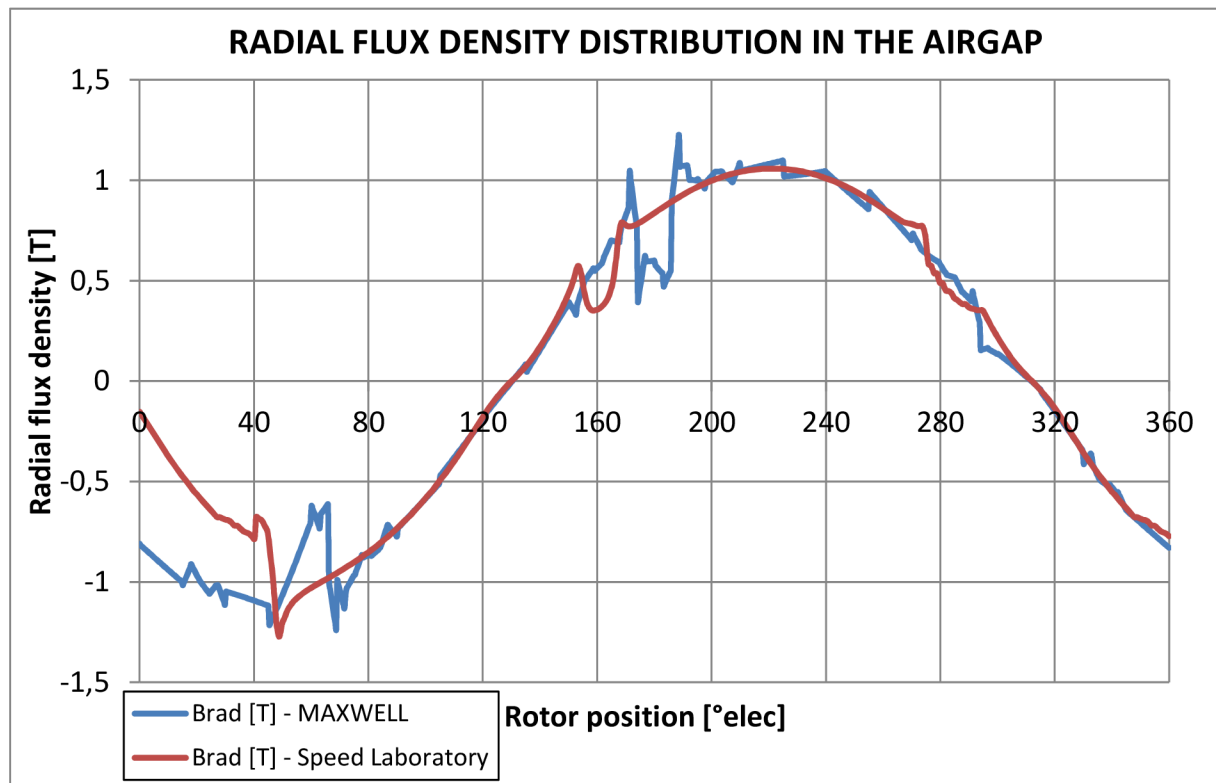
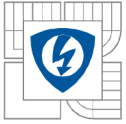


Fig 25.: Radial flux density distribution in the air gap

The oscillation is also affected by stray flux, which oversaturated the corners of each stator teeth, as shows Fig 23.



4.4.2 Tangential flux density distribution in the air-gap

The second of these basic components of the flux-density in the air gap is the tangential component. Tangential flux-density distribution shows the Fig 26. The curve of B_{tg} is also affected by geometry of stator teeth, and slots shape. The value of B_{tg} is calculated by equation (4.12).

$$B_{tg} = -B_x \sin \theta + B_y \cos \theta \quad (4.12)$$

Example of calculation B_{tg} for the rotor position angle $\theta = 253^\circ$ is shown in equation (4.13) :

$$B_{tg} = -0,308 \cdot 0,45 + 0,122 \cdot 0,893 = -0,0448 T \quad (4.13)$$

The oscillations in Fig 26 are also affected by stray flux, which oversaturated the corners of each stator teeth, as shows the detail in Fig 23.

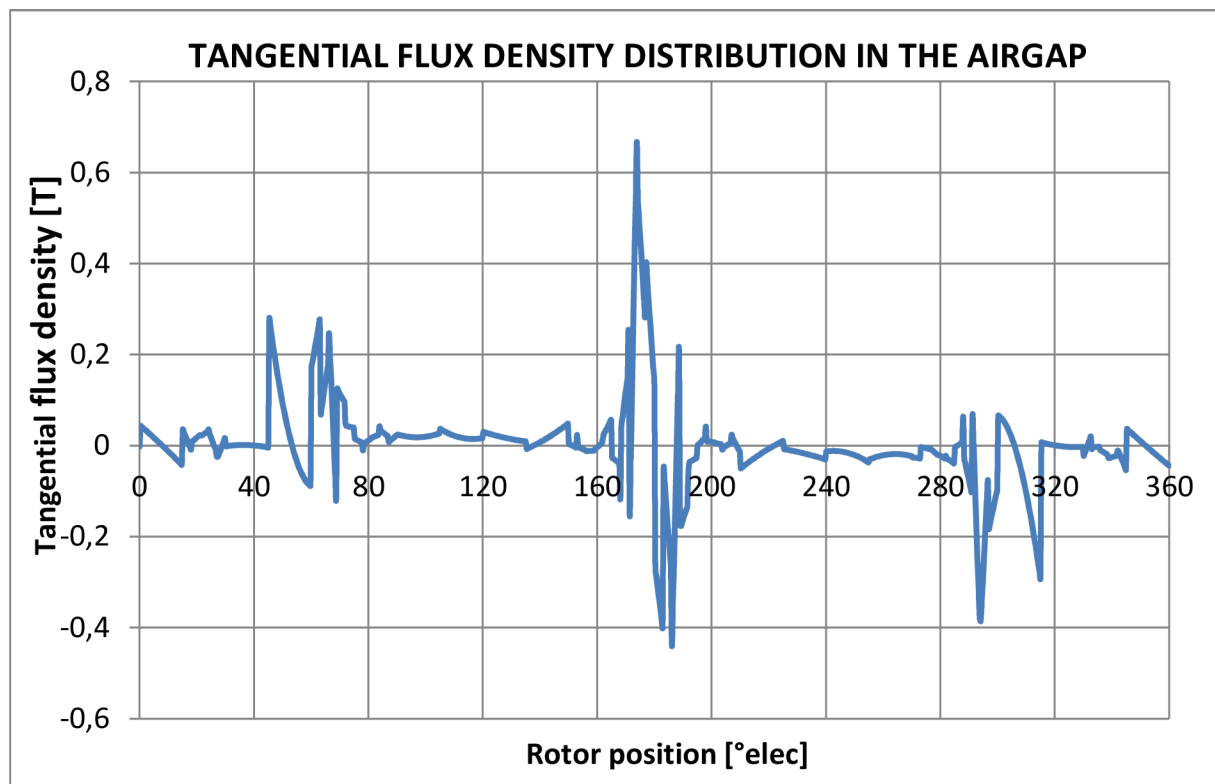
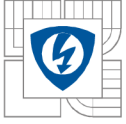


Fig 26.: Tangential flux density in the air gap

4.5 Iron Losses

Core loss or iron loss is a form of energy loss which happens in electrical transformers and other inductors. Two types of iron loss are hysteresis loss and eddy current loss. The hysteresis is well known in ferromagnetic materials which the relationship between magnetic-field strength (H) and magnetic flux density (B). The hysteresis loss results from the friction between the magnetic domains. Eddy current loss occurs when the rotating magnetic field induces alternating current, called eddy



current, in the iron core. The eddy current loss can be minimized by making the core with thin sheets or laminate sheets of magnetic material [17]

For a sinusoidal magnetic flux density B , the iron loss power density is given by:

$$\Delta P_{IRON} = \Delta P_h + \Delta P_c + \Delta P_e \quad (4.14)$$

Where hysteresis loss ΔP_h is:

$$\Delta P_h = k_h f B_{fm}^\beta \quad (4.15)$$

Classic eddy current loss ΔP_c is:

$$\Delta P_c = k_c (f B_{fm})^2 \quad (4.16)$$

Excess loss ΔP_e is:

$$\Delta P_e = k_e (f B_{fm})^{1,5} \quad (4.17)$$

Where:

f	Frequency of magnetic flux waveform
B_{fm}	Peak of the sinusoidal density
β	Steinmetz constant
k_h	Hysteresis constant
k_c	Eddy current constant
k_e	Excess loss constant

Simulation conditions in the simulation of core losses as follows are observed. Model is simulated by using of the transient setup. Zero currents to windings and magnets are set as the excitations. The rotor speed is set 3000 rpms in motion setup. Material for the stator and rotor to calculation of losses is set. Core losses waveform was determined for the selected mesh5 (Fig 10). Simulation runs only on one quarter of the machine but value is evaluated for the whole machine.

In this work only the iron losses were evaluated. The course of losses of synchronous machine with the surface mounted permanent magnets on the rotor is shown in Fig 27. The material of stator and rotor is M19_24 steel as shown in enclosure A1. The average value of core losses in the simulation is 204.5 W. The losses resulting curve is based on the equations (4.14), (4.15), (4.16) and (4.17).

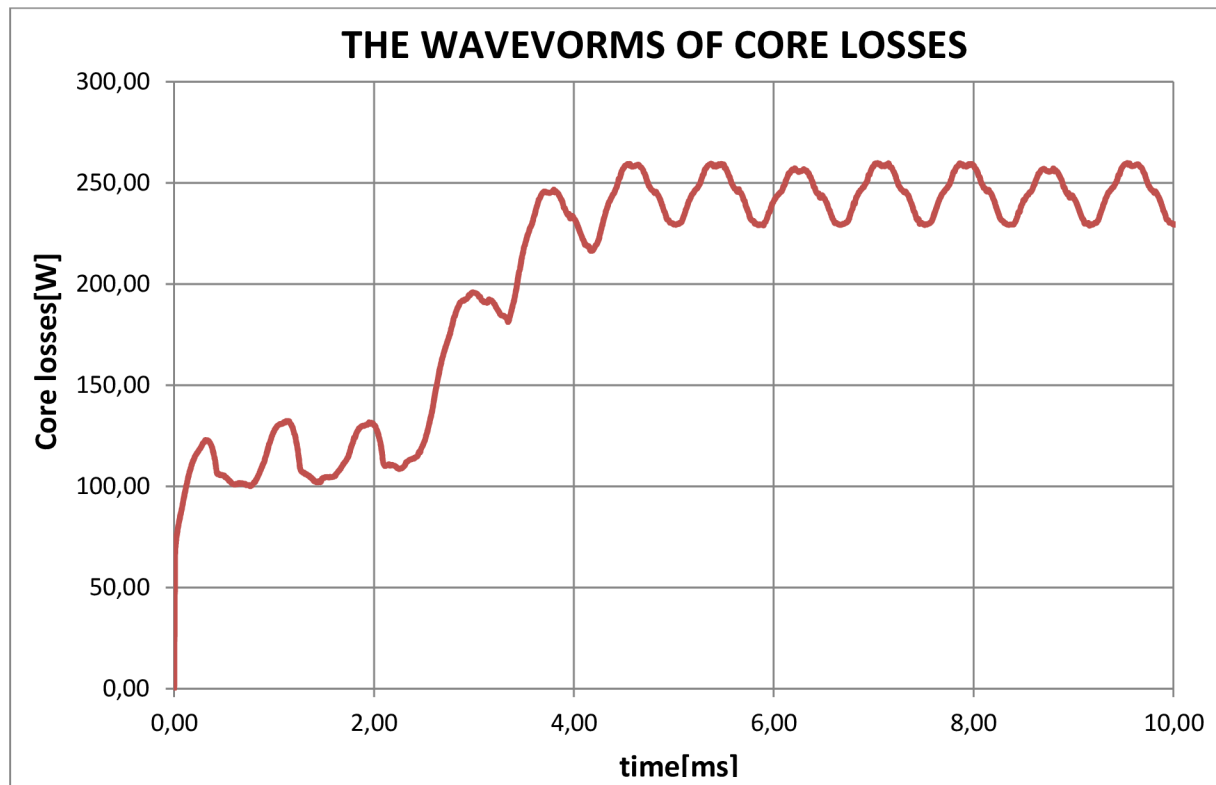
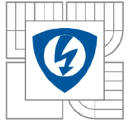


Fig 27.: Core losses waveform.

Hysteresis losses are directly proportional to the speed of the machine. Eddy current losses are proportional to the square of the speed. For this reason, the course of the iron losses stabilizes on the displayed value.

Analytical calculation of core losses from material M19_24 properties is evaluated. Materials properties are shown in enclosure A1. Values of hysteresis and eddy current constant are converted to the weight of the material. Analytical value of iron losses is:

$$\Delta P_{IRON} = \Delta P_h + \Delta P_c + 0 = 174,9 + 58,6 = 233,7W \quad (4.18)$$

Where hysteresis loss ΔP_h is:

$$\Delta P_h = 0,78 \cdot 200 \cdot 1,1^{1,2} = 174,9W \quad (4.19)$$

Value of Steinmetz constant is selected according to literature.[18] Classic eddy current loss ΔP_c is:

$$\Delta P_c = 0,00121 \cdot (200 \cdot 1,1)^2 = 58,6W \quad (4.20)$$

Excess loss ΔP_e value is zero, because excess loss constant is not set in material definition.

Average core loss values for both used PM materials is shown in Table 4.4.

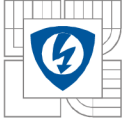


Table 4.4: Core losses values for different permanent magnet material.

Permanent magnets material	$\Delta P_{IRON} [W]$
NdFeB	204,5W
SmCo	232,05W
Analytically calculated	233,7W

Comparison between core losses waveforms using different PM material is shown in Fig 28. Differences in curves are given by different permanent magnets properties. Waveforms were obtained from the simulation at 125 ° C.

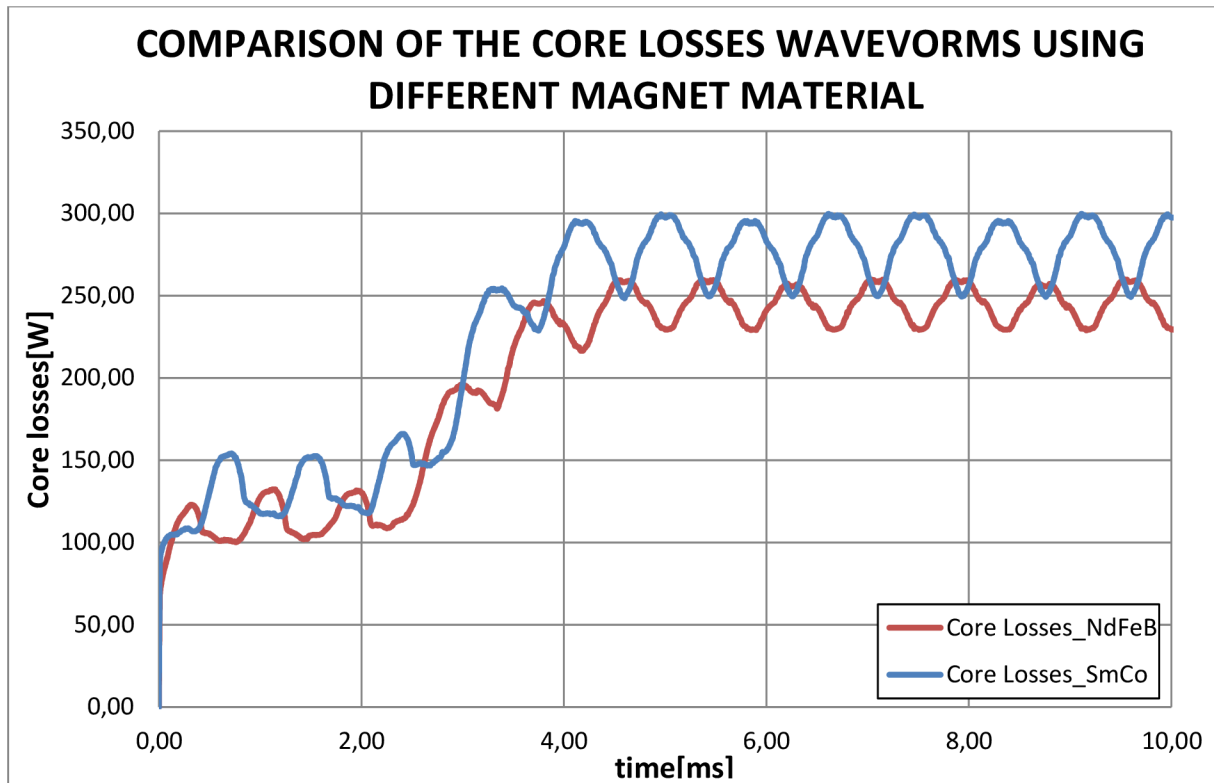


Fig 28.: Comparison of core losses waveforms using different magnet material

4.6 Solid losses

Solid losses are losses in magnets per revolution. Value of solid losses is influenced by the material of permanent magnets. Values of these losses are known from FEM simulation in Maxwell. In FEM simulation the values of solid losses represent losses in whole rotor. Value of these losses is important for machine efficiency calculation [9]. The waveform of solid losses for NdFeB magnets is shown in Fig 29.

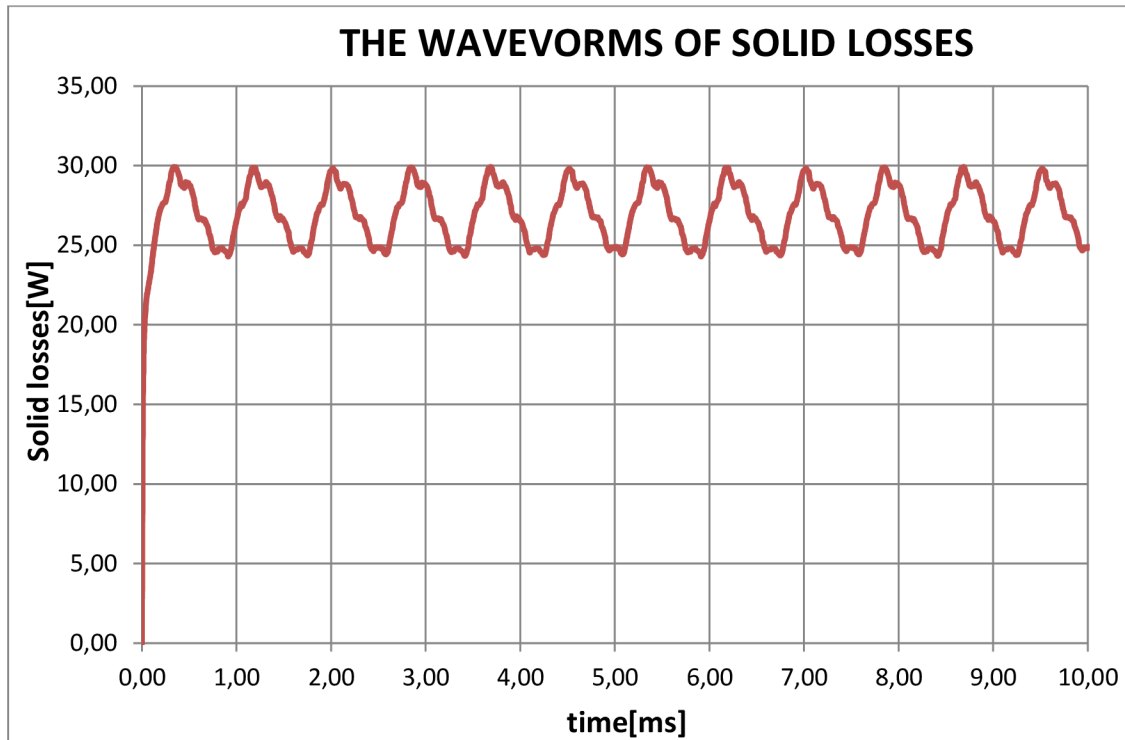
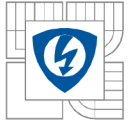


Fig 29.: Solid losses waveformss for NdFeB magnets.

For the calculation of machine efficiency, the waveforms for both PM magnet materials are evaluated. Average values of solid losses are in Table 4.5. Comparison of solid losses waveforms for both PM materials is shown in Fig 30

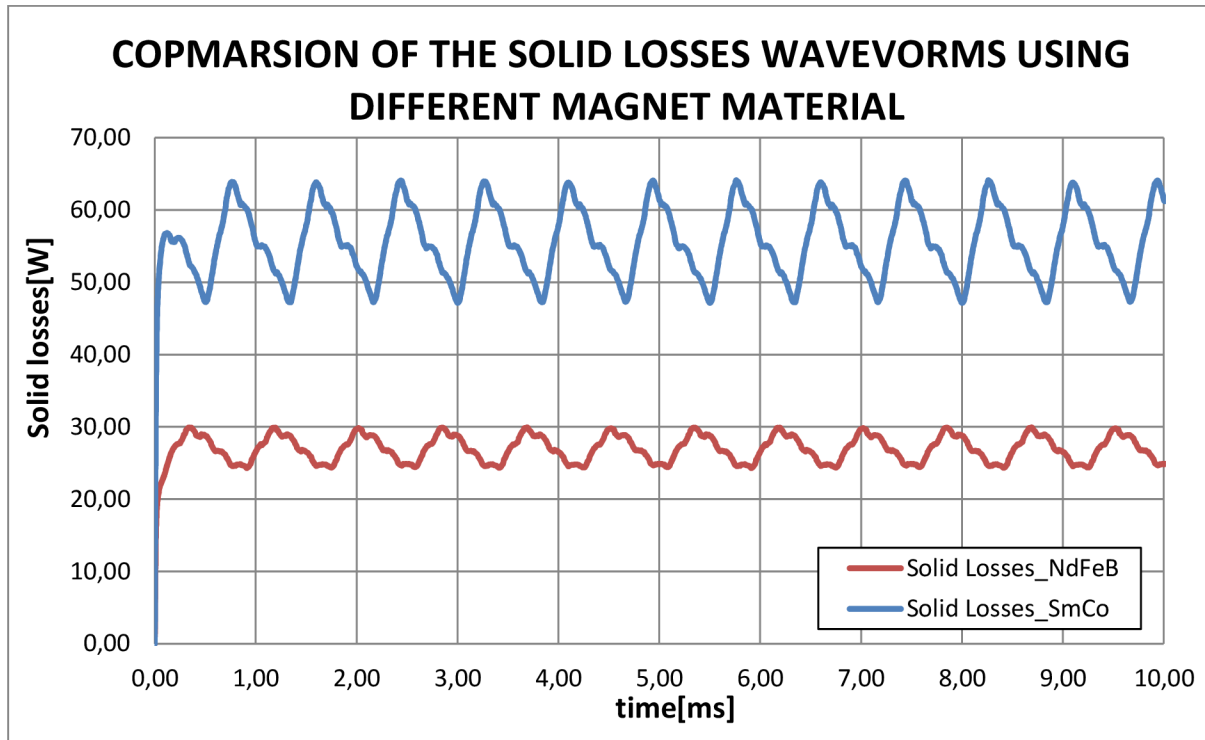


Fig 30.: Comparison of solid losses waveforms for both PM materials.

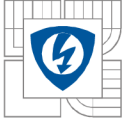


Table 4.5: Values of solid losses.

PM material	$\Delta P_{MAG} [W]$
NdFeb	26,9W
SmCo	55,5W

4.7 Calculation of machine inductances

The d -axis and q -axis inductances have an important influence on both the steady-state and dynamic performance of permanent magnet (PM) brushless ac machines. Calculation of machine inductances for original NdFeB magnets is performed in this chapter.

Their accurate prediction is essential, not only for predicting performance aspects such as the torque and flux-weakening capabilities, but also for designing control systems, in order to maximize the efficiency, power factor, etc. The influence of magnetic saturation is usually accounted for by determining current-dependent inductances and, however, since high local saturation may occur due to the combined influence of the PMs and the armature reaction field, especially in interior-magnet rotor machines, analytical methods for determining the winding inductances are often inadequate, and a numerical method must be employed. [13]

Simulation conditions are observed in the simulation of machine inductances as follows. Model is simulated by using magneto-static setup. Input phase currents to windings are set for each time manually. Values of currents are sinusoidal. Nominal value of the phase current is $I_{RMS,abc}=25,8A$. The values of inductances are evaluated for 5 different times and two special cases. The whole machine is simulated. Flux-linkage distribution in the machine geometry is shown.

The aim of this chapter is to determine the d -axis and q -inductance. From results given by simulations of a parametric model the values of inductances are calculated. Simulations were performed using magneto-static simulation in Maxwell. For comparison of the inductances 7 values are calculated. The output from the simulation is value of phase flux-linkage. These phase values in the Table 4.7 are converted using Clark's transformation into the coordinate system of $\alpha\beta$ (attached to the stator) by equations (4.21) and (4.22), and then to the dq -coordinate system (attached to the rotor) by equations (4.23) and (4.24). Values of input current are shown in Table 4.6.

$$i_a = i_\alpha \quad (4.21)$$

$$i_\beta = \frac{i_b - i_c}{\sqrt{3}} \quad (4.22)$$

$$i_d = i_\alpha \cos \theta + i_\beta \sin \theta \quad (4.23)$$

$$i_q = -i_\alpha \sin \theta + i_\beta \cos \theta \quad (4.24)$$

Where θ is actual transformation rotation angle of rotor to stator. For this case is: $\theta = 7,5^\circ$

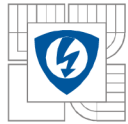


Table 4.6: Input currents values

	t_1	t_2	t_3	t_4	t_5	$I_d=0, I_q=MAX$	$I_q=0, I_d=MAX$
$i_a[A]$	0,0000	36,4867	31,9736	17,5776	-36,4867	-4,5730	36,1990
$i_b[A]$	31,5984	-18,2434	-31,2094	-36,4787	18,2434	33,6358	-14,1392
$i_c[A]$	-31,5984	-18,2434	-0,7641	18,9011	18,2434	-29,0628	-22,0598
$i_d[A]$	4,7625	36,1746	29,4057	13,2538	-36,1746	0	36,4862
$i_q[A]$	36,1746	-4,7625	-21,6006	-33,9944	4,7625	36,4862	0

Table 4.7: Values of the calculated inductances.

	t_1	t_2	t_3	t_4	t_5	$I_d=0, I_q=MAX$	$I_q=0, I_d=MAX$
$\psi_a[Wb]$	0,0393	1,4881	1,2918	0,6863	-1,4881	-0,1399	1,4102
$\psi_b[Wb]$	1,1662	-0,7100	-1,2215	-1,4273	0,7100	1,2429	-0,5226
$\psi_c[Wb]$	-1,2054	-0,7787	-0,0704	0,7413	0,7787	-1,1031	-0,8880
$\psi_\alpha[Wb]$	0,0393	1,4881	1,2918	0,6863	-1,4881	-0,1399	1,4102
$\psi_\beta[Wb]$	1,3692	0,0397	-0,6646	-1,2521	-0,0397	1,3545	0,2110
$\psi_d[Wb]$	0,2176	1,4805	1,1940	0,5170	-1,4805	0,0381	1,4257
$\psi_q[Wb]$	1,3524	-0,1549	-0,8275	-1,3309	0,1549	1,3611	0,0251
$L_d[H]$	0,0457	0,0409	0,0406	0,0390	0,0409	0,003	0,0391
$L_q[H]$	0,0374	0,0325	0,0383	0,0392	0,0325	0,0373	0,003

Calculation example, Table 4.7: L_d for time t_1 , L_q for time t_3 . Values of currents are from Table 4.6.

$$L_d = \frac{\psi_d}{i_d} = \frac{0,2176}{4,7625} = 0,0457H$$

$$L_q = \frac{\psi_q}{i_q} = \frac{1,3524}{36,1746} = 0,0374H$$

Simulations were performed in magneto-static mode for different times. Currents in windings are electrically shifted in time. For specified values of current in the windings, have been calculated phase flux-linkages from them subsequently calculated values of inductances. Magnets are set as non-model object for the simulations.

The calculated values of inductances for times t_1 , t_2 , t_3 , t_4 and t_5 are shown in Fig 31. Inductance values are periodic, with an additional period of power supply current, values are repeated.

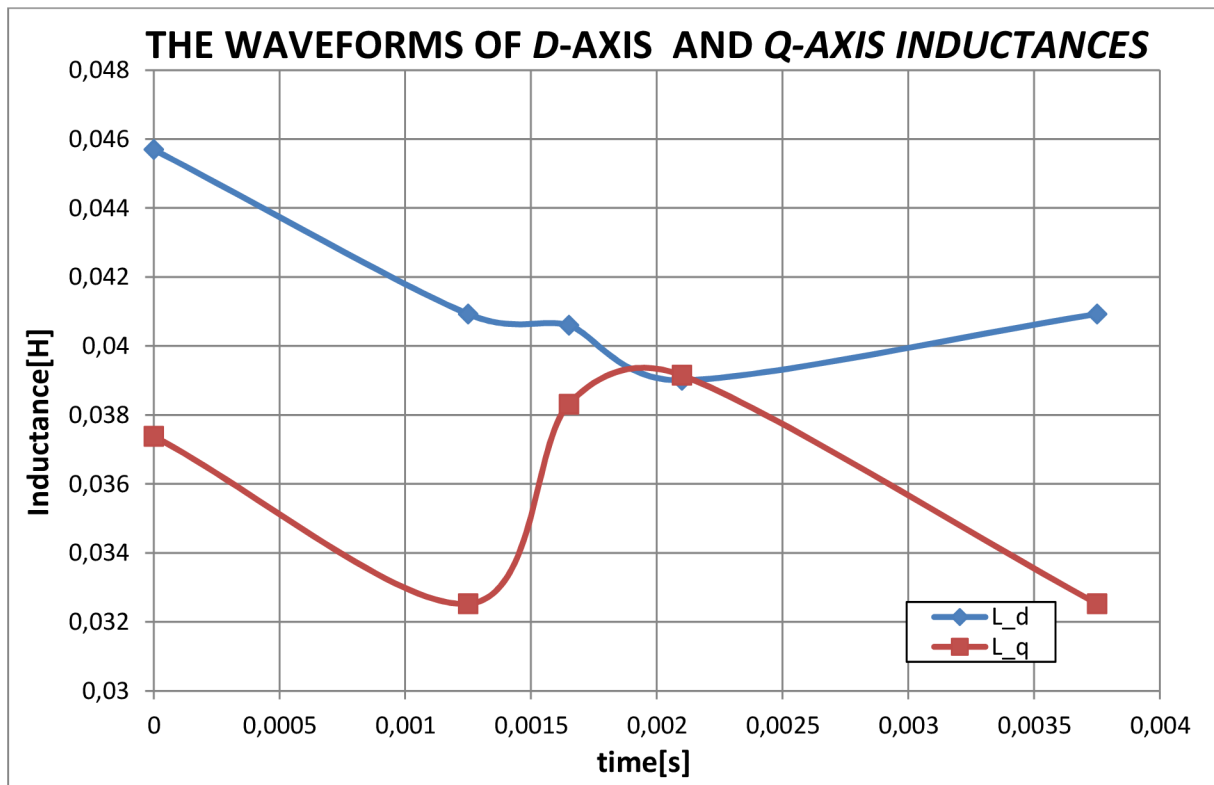


Fig 31.: The waveforms of machine inductances

Flux-linkage distribution for different values of currents in time, are shown in Fig 32, Fig 33, Fig 34. From flux-linkage distribution in geometry of the machine currents sizes in *d*-axis and *q*-axis are apparent. In Fig 33 and Fig 34 two special cases are shown. Fig 33 shows the situation when the zero current in *d*-axis and in the *q*-axis current is maximal. In the Fig 34 the reverse case is shown.

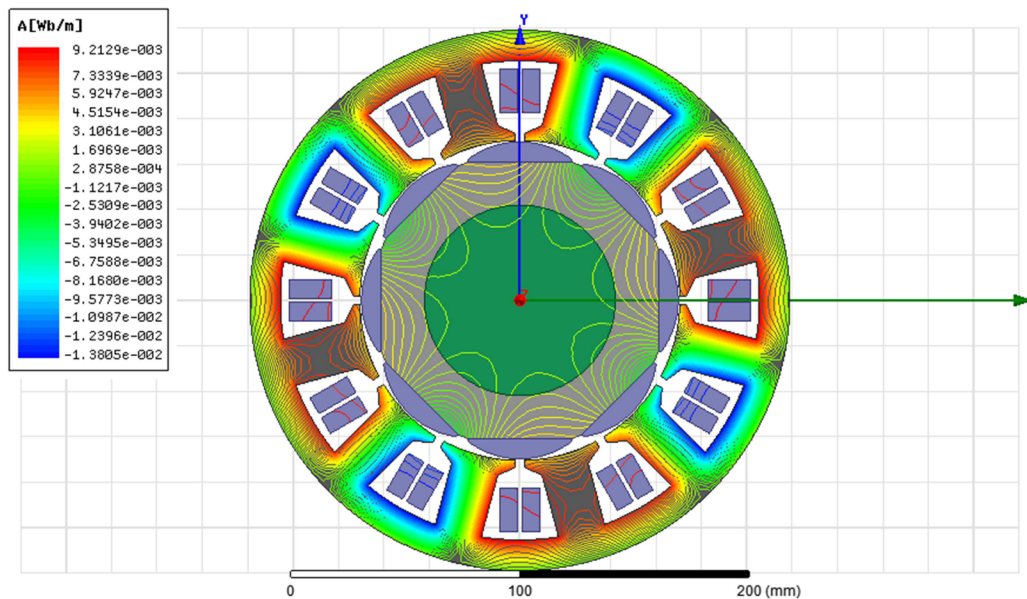


Fig 32.: Flux-linkage distribution in machine geometry for first-time simulation.

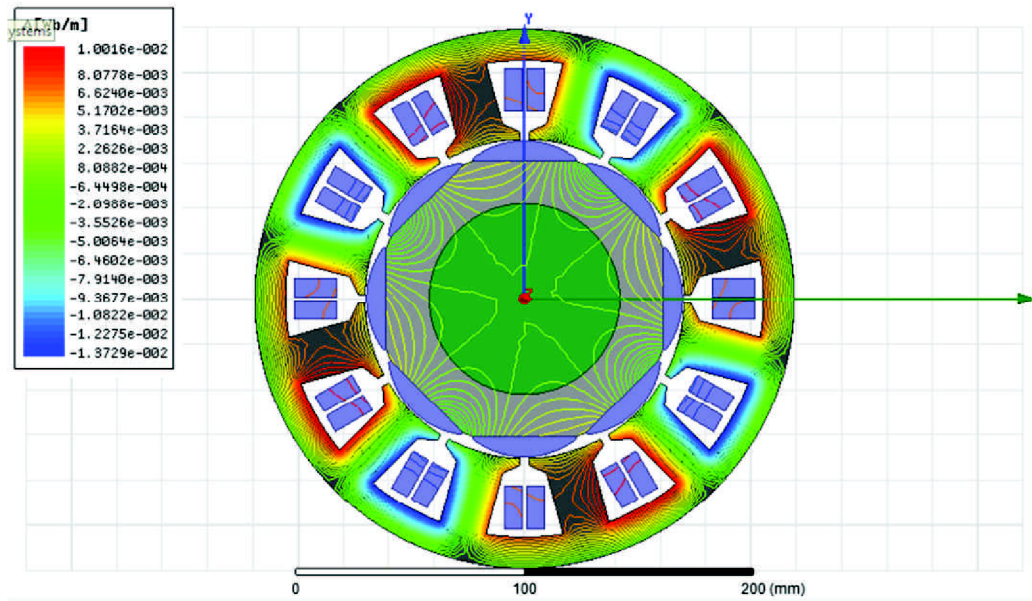
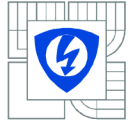


Fig 33.: Flux-linkage distribution in machine geometry for condition $i_d=0$, $I_q=MAX$.

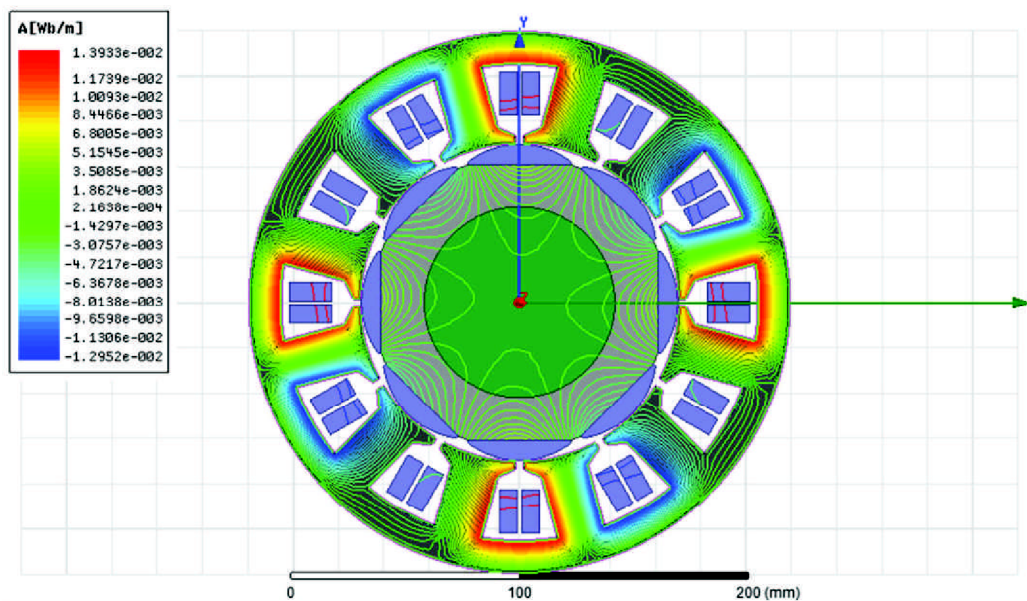
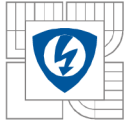


Fig 34.: Flux-linkage distribution in machine geometry for condition $I_d=MAX$, $I_q=0$.

Flux-linkage distribution for two special cases is shown in Fig 33 and Fig 34. These two cases are shown purposely. From flux-linkage distribution currents sizes in dq -axes are apparent. Current size affects the value of flux creating component and torque creating component in torque equation (4.25):

$$T = \frac{3}{2}p(\Psi_d i_q - \Psi_q i_d) \quad (4.25)$$



4.8 Demagnetization analysis of original NdFeB Permanent Magnets

A permanent magnet is an essential part of modern electrical machine, which means that the PM material should be modelled properly. A good model should describe accurately each possible working point in second and third quadrant of hysteresis plane.

In present models of a PM machine, the permanent magnet material is usually modelled with two parameters only: remanence B_r and recoil permeability. In some cases, instead of remanence, the normal coercivity H_c of material is used. [15]

These parameters lead to a linear model that does not take into account the possibility of demagnetisation. Normally this is not a problem because PM machines should be designed so that the risk of demagnetisation is avoided even in some hazard situations like short circuits. However, if behaviour of machine after demagnetisation needs to be modelled a more sophisticated PM model is required.

Modern PM Materials includes ferrites, Rare Earth material and different plastic bonded materials. Most of these materials except some plastic bonded materials show almost linear behaviour up to the demagnetisation limit.

In hard magnetic materials the second quadrant of hysteresis is most important and is called demagnetization curve. Demagnetization curves as well as the other quadrants of hysteresis can be drawn both in the $J(H)$ picture as well as in the $B(H)$ description. This is also the case in Fig 35, which supplies those basic parameters of the demagnetization curve, which are mainly used in technical literature about permanent magnets. [16]

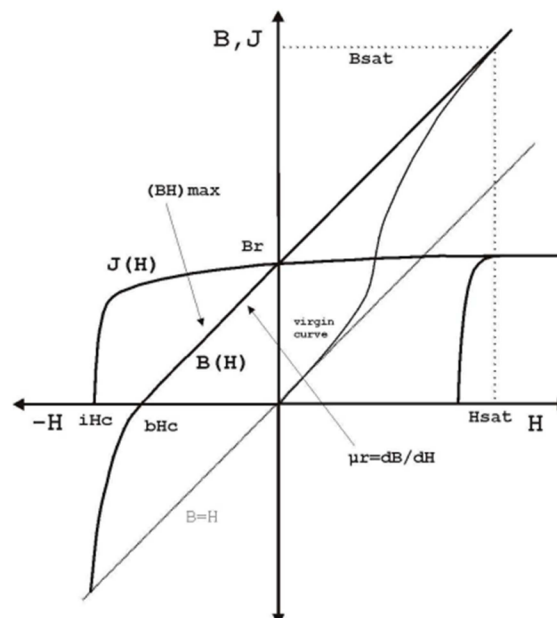
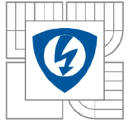


Fig 35.: The second quadrant of demagnetization curve defines the basic parameters [16]



Where is:

B_r	Remanence induction [T]
bH_c	Coercitivity of J [A/m],
jH_c	Coercitivity of B [A/m]
μ_r	Recoil permeability [-]
$(BH)_{max}$	Maximum energy product [kJ/m ³]

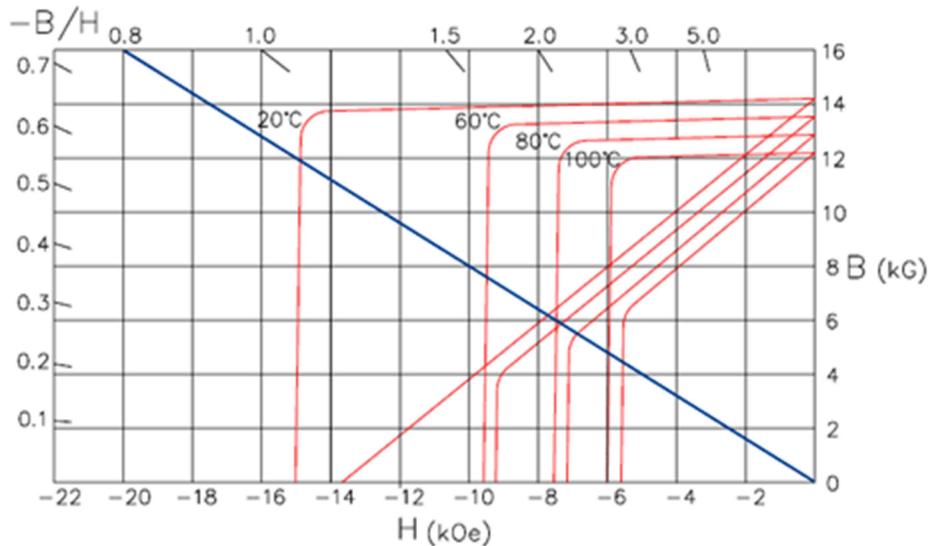
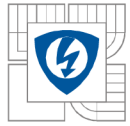


Fig 36.: Example of demagnetization characteristic for PM magnets at different temperatures [15]

Diagonal red line is the demagnetization curve in Fig 36. Notice that each of the diagonal lines has a bend in it, colloquially referred to as the “knee” in the curve. If the blue line, which shows the working condition of the magnet, crosses above the knee in the curve, then the magnet is operating in its safe linear region and should perform as expected. If the magnet’s load line is below the knee on the curve, the magnet will become demagnetized and damaged. It is also important to notice that the knee gets higher with increasing temperatures, which reflects the material’s increasing predisposition to demagnetization at higher T. [14]

Simulation conditions are observed in the demagnetization analysis as follows. Model is simulated by using magneto static setup. Input phase currents to windings are set for each time manually. Values of currents are sinusoidal. Curve is found for no-load condition and for given load condition. In the simulation smallest values of B and H in the magnet surface are determined, which are subsequently evaluated. From the observed values demagnetization curves in Fig 37 are compiled.

In this work material for permanent magnets called *SUMMITOMO* is used, marked as ATMAXEH33. BH curve of this material is shown Fig 43 in Enclosure B1. Demagnetization analysis for 125°C was performed. Input current was elected as five time bigger then nominal current, for demagnetizing analysis. In Fig 37 the demagnetisation curves for 20°C a 125°C are shown. For



temperature 125°C demagnetization knee was determined. Selected current did not cause demagnetization.

Table 4.8: Values for plotting the demagnetization curves

Demagnetization Curves						
20C Demag Line			Demag Knee Point for		125	Celsius
Br (T)	Hc (kA/m)	slope	B (T)	H (kA/m)	B (T)	Hc (kOe)
1,128	-900	0,00125	-0,31251	-1042,5	1,02	-15,21
Demagnetization Curves						
20C Demag Line			Demag Knee Point for		125	Celsius
Br (kG)	Hc (kOe)	slope	B (kG)	H (kOe)	B (kG)	Hc (kOe)
11,28	-11,3098	1,00	-3,12	-13,10052	9,95	-9,97
Fig 37.	FEA No Load		FEA Load			
	B (T)	H (a/m)	B (T)	H (a/m)		
	0,68718	-636456	0,0065	-917440		

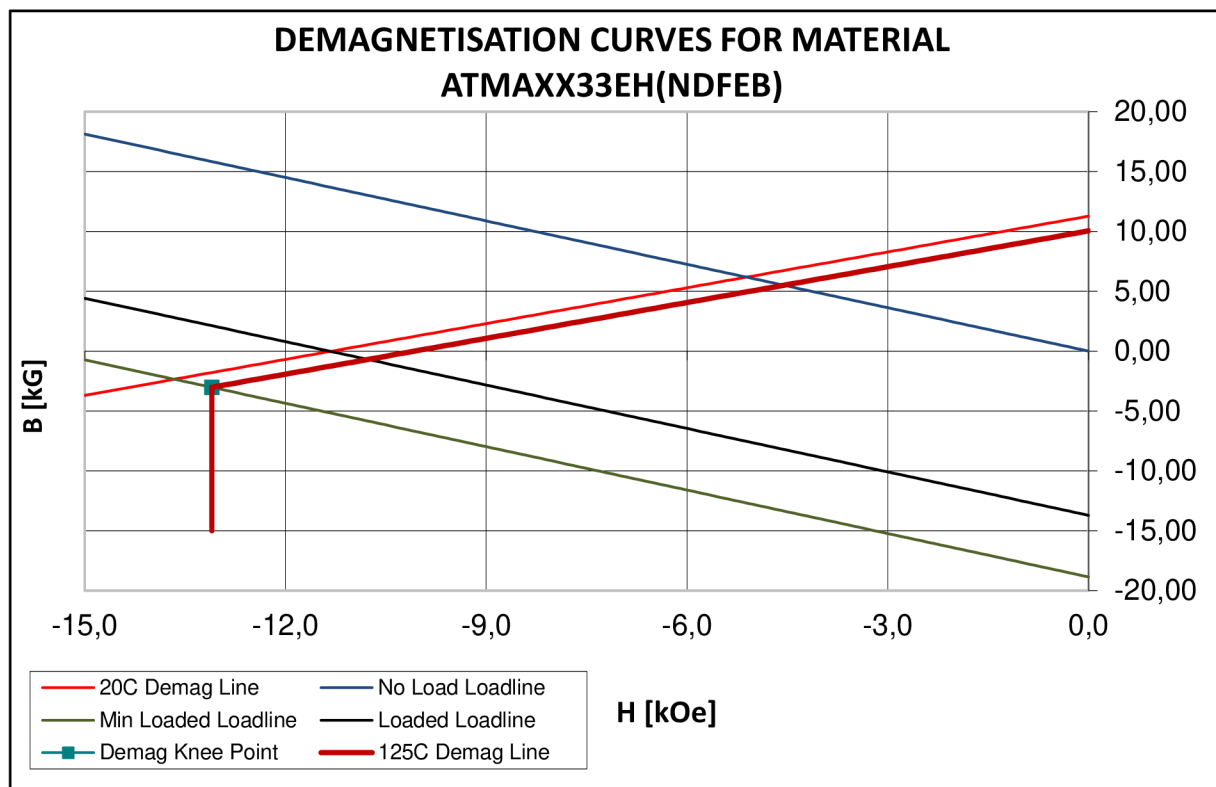
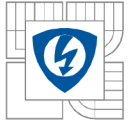


Fig 37.: Demagnetisation curves for magnet material ATMAXX33EH(NdFeB).

Better performance in higher temperatures is known from the material parameters for SmCo PM. SmCo magnets operate at temperatures up to 350 ° C while NdFeb magnets operate at temperature up to 220°C. This is the reason why the demagnetization analysis was not performed. The demagnetization knee for SmCo magnets is reached with higher current then five time nominal value.

Demagnetization analysis is very complex and time consuming task, therefore, was not in this work further solved.



4.9 Calculation of the machine efficiency

Calculation of machine efficiency is described in this chapter. Machine efficiency shows the correctness of the design. Efficiency of electric machines is a frequently discussed issue that is defined by European directives. In this work is not evaluated inclusion of the simulated machine to a specific class of these directives. Typical power flow diagram of permanent magnet synchronous motor is shown in Fig 38.

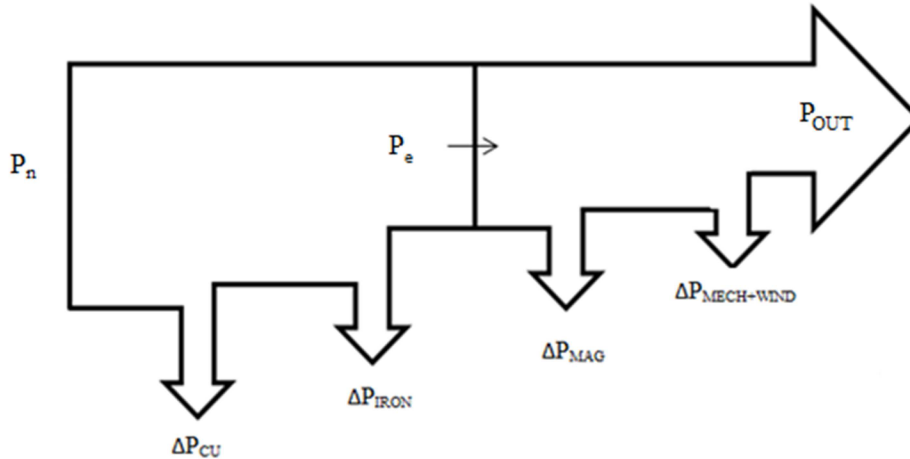


Fig 38.: Power flow of PMSM[21]

Calculation of efficiency is done using several different simulations with different simulation conditions. Results of each simulation are evaluated in the previous chapters. From these results the value of efficiency is calculated by equations (4.26), (4.27) and (4.30). Efficiency of the machine for both used PM material is shown in Table 4.9. For both PM material is efficiency calculated from nominal power given by manufacturer.

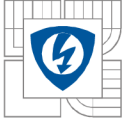
Table 4.9: Calculation of machine efficiency for different Pm material

PM material	P_n [W]	P_{n_FEM} [W]	ΔP_{Cu} [W]	ΔP_{IRON} [W]	ΔP_{MAG} [W]	ΔP_{M+W} [W]	η [%]
NdFeB	14400	13492,4	124,6	204,5	26,9	432	88,2
SmCo	14400	14305,3	124,6	232,05	55,5	432	93,5

Calculation of windings losses ΔP_{Cu} for nominal current $I_{RMS} = 25,8A$ is given by equation (4.26). Value of resistance $R_{Cu} = 0,0624\Omega$ is determined from the model in RMxprt.

$$\Delta P_{Cu} = 3 \cdot R_{Cu} \cdot I^2 = 3 \cdot 0,0624 \cdot 25,8^2 = 124,6W \quad (4.26)$$

From chapters 4.5 and 4.6 the values of iron and solid losses for both used permanent magnets material are known. Values of these loses are shown in Table 4.4and Table 4.5.



Value of inner electromagnetic performance is calculated from steady torque M_e , shown in Table 4.3, and angular velocity ω in equation (4.27).

$$P_{e_FEM_NdFeB} = M_{e_NdFeB} \cdot \omega = 41,9 \cdot \frac{2\pi \cdot 3000}{60} = 13163,3W \quad (4.27)$$

Nominal value of performance from FEM simulation is calculated in equation (4.28).

$$P_{n_FEM_NdFeB} = P_{e_NdFeB} + \Delta P_{Cu} + \Delta P_{IRON_NdFeB} \quad (4.28)$$

$$P_{n_FEM_NdFeB} = 13163,3 + 124,6 + 204,5 = 13492,4W \quad (4.29)$$

Value of mechanic and wind losses ΔP_{M+W} is chosen as 3% of rated power specified by manufacturer, $P_n = 14,4kW$.

Efficiency of the machine is given by equation (4.30).

$$\eta_{NdFeB} = \frac{P_{n_NdFeB} - \Delta P_{Cu} - \Delta P_{IRON} - \Delta P_{MAG} - \Delta P_{M+W}}{P_n} \cdot 100 \quad (4.30)$$

$$\eta_{NdFeB} = \frac{13504,6 - 124,6 - 204,5 - 26,9 - 432}{14400} \cdot 100 = 88,2\% \quad (4.31)$$

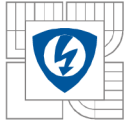
Values of efficiencies are given by calculation from electromagnetic performance given by steady torque. In this work the value of steady torque is not evaluated with using a vector control. If vector control of the machine is used, higher value of steady torque is reached. Vector control is not used in this thesis. Without vector control of the machine is value of nominal power from finite element method simulation lower than nominal value specified by the manufacturer.

5 Maxwell optimization analyses

In Maxwell software is an option to perform the optimization. Users can choose from five different methods of optimization. Each method is working with different algorithm. Conducting an optimization analysis allows user to determine an optimum solution for his problem.

All five optimizers assume that the nominal problem he is analysing is close to the optimal solution; therefore, he must specify a domain that contains the region in which he expected to reach the optimum value. All five optimizers allow user to define a maximum limit to the number of iterations to be executed. This prevents him from consuming his remaining computing resources and allows him to analyse the obtained solutions. From this reduced range, user can further narrow the domain of the problem and regenerate the solutions.

All optimizers also allow him to enter a coefficient in the Add Constraints window to define the linear relationship between the selected variables and the entered constraint value. For the sequential nonlinear programming (SNLP) and sequential mixed integer nonlinear programming (SMINLP)



optimizers, the relationship can be linear or nonlinear. For the Quasi Newton and Pattern Search optimizers, the relationship must be linear. [20]

5.1 Genetic Algorithm

Genetic Algorithm (GA) optimizers are part of a class of optimization techniques called stochastic optimizers. They do not use the information from the experiment or the cost function to determine where to further explore the design space. Instead, they use a type of random selection and apply it in a structured manner. The random selection of evaluations to proceed to the next generation has the advantage of allowing the optimizer to jump out of a local minimum at the expense of many random solutions which do not provide improvement toward the optimization goal. As a result, the GA optimizer will run many more iterations and may be prohibitively slow. [20]

5.2 Pattern Search

If the noise is significant in the nominal project, use the Pattern Search optimizer to obtain the results. It performs a grid-based simplex search, which makes use of simplifies: triangles in 2D space or tetra-hedra in 3D space. A simplex is a Euclidean geometric spatial element having the minimum number of boundary points, such as a line segment in one-dimensional space, a triangle in two-dimensional space, or a tetrahedron in three-dimensional space. [20]

5.3 Quasi Newton

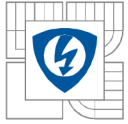
If the Sequential Non Linear Programming Optimizer has difficulty, and if the numerical noise is insignificant during the solution process, use the Quasi Newton optimizer to obtain the results. The Quasi Newton optimizer works on the basis of finding a minimum or maximum of a cost function which relates variables in the model or circuit to overall simulation goals. The user defines one or more variables in the problem definition and a cost function in the optimization setup. The cost function relates the variable values to field quantities, design parameters like force or torque, power loss, etc. The optimizer can then maximize or minimize the value of the design parameter by varying the problem variables. [20]

5.4 Sequential mixed integer nonlinear programming (SMINLP)

The Sequential Mixed Integer Nonlinear Programming (SMINLP) optimizer is equivalent to the SNLP optimizer with only one difference. Many problems require variables take only discrete values. One example might be to optimize on the number of turns in a coil. To be able to optimize on number of turns or quarter turns, the optimizer must handle discrete optimization variables. The SMINLP optimizer can mix continuous variables among the integers, or can have only integers and works if all variables are continuous. The setup resembles the setup for SNLP, except that you must flag the integer variables supporting integer variables. You can set up internal variables based on the integer optimization variable. [20]

5.5 Sequential nonlinear programming (SNLP)

The main advantage of SNLP over Quasi Newton is that it handles the optimization problem in more depth. This optimizer assumes that the optimization variables span a continuous space. As a result, there is no Minimum Step Size specified in this optimizer and the variables may take any value within the allowable constraints and within the numerical precision limits of the simulator. Like Quasi



Newton, the SNLP optimizer assumes that the noise is not significant. It does reduce the effect of the noise, but the noise filtering is not strong. [20]

6 Performed optimization with respect to the highest possible efficiency

The aim of this chapter is to increase efficiency of the machine with using optimization. In chapter 5 the Maxwell optimization methods are described. Many different optimization methods are used by manufacturers to increase machine's properties. Procedure of optimization in Ansoft Maxwell is described in next subchapters.

Main task of optimization in this thesis is to increase machine efficiency by changing dimensions of magnets. Several variations of PM dimensions are set and evaluated.

6.1 Selected optimization method

From five optimization methods which can be used in Maxwell the Generic algorithm is selected. Disadvantage of optimization without external programming software is a several different simulations must be done for evaluation of machine efficiency. This problem is eliminated if the aim of optimization is not complex as calculation of machine efficiency. For example the minimalizing of cogging torque only one model simulation is used. For this model is set optimization problem. In options the optimization goal is set. Parameters and their limits are set. Maxwell runs simulation and finds the best possible result based on the optimization settings.

Maxwell with external software is used very often. One of this software is Matlab. From Matlab the models in Maxwell are managed. With this software combination complex optimization tasks can be solved easily. In this work only Ansoft Maxwell optimization is used.

6.2 Performed optimization

Optimization with generic algorithm was set and started. Results of the optimizations not correct with insufficient user experience. The results of the optimization are evaluated. Wrong parameter limits resulting to long time of simulation. From results proportions of magnets is shown in Fig 39. Optimization result is maximum value of parameter $offsRmo = 36,238$ mm.

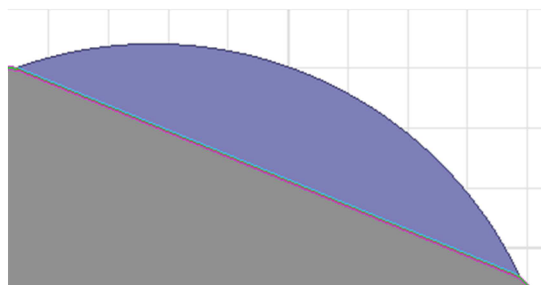
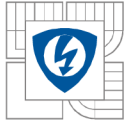


Fig 39.: PM dimensions from optimization.



Demagnetization on both sides is caused by dimensions of the magnet. Magnets with this dimensions is not possible to manufacture.

For this reason and time requirements manual optimization is performed. The original dimensions of the machine and the other 4 variants of selected PM parameters are proposed in Table 6.1.

Four different variants of PM parameters are shown in Table 6.1. Comparison to original dimensions is shown. Simulations for evaluation of efficiency are performed for each variant. Simulations are described in chapter 4. Combinations of parameters LM, wMag, offsRmo are set manually to each simulation model. Created parametric model is used. Change of parameter is very easy and fast with parametric model. Parameter variations are generated randomly by user.

Table 6.1: Values of parameters in performed optimization.

Variant	LM[mm]	wMag[mm]	offsRmo[mm]
Original	8,848	45,3473	31,801
1	8,348	47,3473	27,801
2	8,448	49,3473	22,801
3	8,848	49,3473	22,801
4	8,848	47,3473	27,801

Simulation of stable torque and core losses are performed for each variation of parameters. Manual optimization without using Maxwell optimization module is performed. Optimization results are evaluated in chapter 7 where machine efficiency is calculated for each variation of parameters.

7 Evaluation of optimization results, comparison with the original machine

For each variant of PM dimensions, shown in Table 6.1, the machine efficiency is calculated. Results for all variant of dimensions are shown in Table 7.1. Values in Table 7.1 are obtained by simulations on parametric model. Manually optimization is performed because Maxwell optimization methods are not very useful without an external program and low experience with the correct settings. From results shown in Table 7.1 the increasing of machine efficiency is obvious. Value of efficiency is increased by increasing of steady torque especially.

Best efficiency $\eta = 96,8\%$ is calculated for PM dimensions variant number three. In comparison to original machine, variant number one, there is the same height of magnet but bigger width. This has resulted to smaller circular arc radius of outer face of the magnet (parameter *offsRmo*, Fig 6, Table 3.3) because of the possibility to manufacture the magnet. With wider magnets the pole arc BetaM is increased.

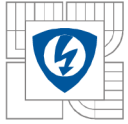


Table 7.1: Results of performed optimization

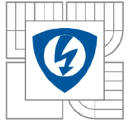
Variation	P_n [W]	P_{n_FEM} [W]	ΔP_{IRON} [W]	ΔP_{Cu} [W]	ΔP_{MAG} [W]	ΔP_{M+W} [W]	η [%]
Original	14400	14305,3	232,05	124,6	55,5	432	93,5
1	14400	14204,6	242	124,6	50	432	92,8
2	14400	14551,4	258,8	124,6	57	432	95
3	14400	14831,1	264,5	124,6	58,3	432	96,8
4	14400	14259,6	249,1	124,6	51,2	432	93,1

For efficiency calculation the losses values are important. With new dimensions of magnets losses are calculated. Value of iron losses is increased. Difference between values for original and new design is 32,45W. The increasing of solid losses is also evident from Table 7.1 but value for new design is higher only by 2,8W.

Higher value of all losses in machine is obtained by optimizing. Difference in values between original and new design of PM is minimal. With new PM bigger value of steady torque is evaluated from simulation on parametric model. In Table 7.2 differences between steady torque values are shown.

Table 7.2: Values of steady torque for original and optimized design.

Selected design	M_e [Nm]
Original design	44,4 Nm
Optimized design	46 Nm



Conclusion

This thesis deals with the possibility of using the finite elements method for the design and analyses of the synchronous permanent magnets machines. The finite elements method is increasingly used for the design of almost all technical devices and their parts. The aim of this work is to discuss the possibility of design the machine more effectively with using the Maxwell software for the simulations.

To analyse and simulation of the synchronous motor with surface mounted magnets on the rotor the finite elements method was used. The results of the simulations, the accuracy of design are evaluated with the original machine designed in the SPEED software.

In the first part of this thesis the traditional machine design approach is described. Some basics requisites and equations are explained. Equations are used for checking the correctness of simulations and design of original machine.

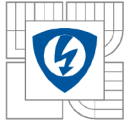
The second part of this work describes the geometry and parameters of parametric model. The basic parameters of the stator, rotor, stator windings and magnets are shown in Table 3.1, Table 3.2, Table 3.3 and Table 3.4. The basic geometry of the motor is shown in Fig 4, Fig 5, Fig 6 and Fig 7.

Materials for the rotor and stator are described by BH curve. The BH curve of stator and rotor steel is shown in enclosure A1. Design of original machine with two different PM materials is simulated. BH curve for NdFeB permanent magnets materials is shown in Enclosure B1. As the new PM material the SmCo magnets are selected. BH curve and material description is shown in enclosure C1.

To analyse of the chosen machine, the parametric model in Ansoft Maxwell was created. Maxwell is the simulation software, which is working with the finite elements method. Maxwell is also having an RMxpert-analytical module. Accuracy of the finite element method depends on the density of the network. In this work three different numbers of elements in the mesh were used. The differences between them are shown in Table 4.1 and the Fig 8, Fig 9, Fig 10..

From the first part of simulations, basic fundamentals, which are important for the correct function of PMSM, were evaluated. The first part of simulations considered no-load condition of the analysed machine. The fundamentals characteristics given by no-load simulations are induced voltage and the distribution of the flux-density in the machine body. In the second part of simulations, the machine was operated in different condition. From the second part of simulations the cogging torque characteristic and the core losses are also calculated.

The next chapter of this work deals with evaluation of the results from simulations of parametric model at no-load. Induced voltage waveforms at different simulation conditions are shown in Fig 11, Fig 12 and Fig 13. The waveforms of the induced voltages compared in Fig 14, shows the differences between RMS values of voltages obtained by different methods. This may be caused by several factors. All the software which is used in this work has own procedure and the specific type of the calculation. The main method for simulations was the finite elements method. To increase the accuracy of the calculation a higher density of points in finite element network is raised. In Fig 15 is shown Comparison between waveforms of induced voltage for original NdFeB and new SmCo magnets is shown in Fig 15. Better performance of SmCo magnets in simulation temperature 125°C is obvious from waveforms.



Individual values of cogging torque are evaluated in Table 4.2. Cogging torque waveforms at different simulation conditions are shown in Fig 16 and Fig 17. Comparison of the waveforms obtained from simulation in different temperatures and finite element network densities is shown in Fig 18. With new PM material cogging torque is also evaluated. Comparison between waveforms for both used PM materials is shown in Fig 19. Bigger value for NdFeB magnets is given by better performance in simulation temperature 25°C.

Values of steady torque are obtained by two different simulations in Maxwell. The torque and windings currents waveforms are the results of simulation in load conditions in Rmxprt. In this simulation, the results are compared with value of torque obtained by other methods. Comparison of all torque values obtained by all methods is shown in Fig 20. As same as induced voltage, the torque is calculated, and his steady value is displayed in detail in Fig 20. The oscillations of the torque around average value are given by ripple and cogging torque. Values of steady torque from simulation on the created parametric model are also evaluated in Fig 22. Comparison between values for both used PM materials is given in Table 4.3. Value of steady torque given by simulation on parametric model is more accuracy because of exact dimensions of the machine.

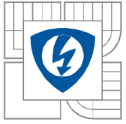
The distribution of flux density on machine body is shown in Fig 23 and Fig 24. The distribution at the no load simulation shows the detail of oversaturated corners in stators tooth. From simulation in load conditions, the possibility to optimize the areas with low saturation is obvious. The flux-density distribution is described by two basic components. The first is the radial flux-density B_{rad} , which is displayed in Fig 25. Second basic component of the air gap flux density is displayed in Fig 26, this component is the tangential flux-density B_{tg} . In both figures waveforms of flux-densities depending on the rotor position are shown. The oscillations of the waveforms are caused by stray flux, shapes and dimensions of the stator slots teeth. The largest deviations in Fig 25, Fig 26 are in places where the pole passes the stator tooth.

Core and solid losses are also calculated in this work. The waveform of core loss is shown in Fig 27. Values for both PM materials is obtained by simulations and shown in Table 4.4. In Table 4.5 values of solid losses is shown. Comparison between waveforms of solid losses for both PM materials is shown in Fig 30.

The distribution of flux density on machine body is shown in Fig 32 and Fig 33 and Fig 34. From values of leakage flux inductances are calculated. Inductances are calculated for different values of inputs currents using the $d-q$ transformation of coordinate systems. In the Fig 31, the waveforms of inductances depending on time are shown. Values of input currents, inductances and fluxes are shown in Table 4.6 and Table 4.7.

Demagnetization analysis for NdFeB magnets is evaluated in chapter 4.5. Demagnetization curves were determined for 25°C and 125°C. Curves are found for the state of no-load, for the selected load. The Fig 37 is shown demagnetization curves. Values for construction of demagnetization curves are shown In Table 4.8. The demagnetization of magnets is not reached for the selected load. Demagnetization analysis for SmCo magnets is not performed because of better performance in higher temperatures. Problem of the demagnetization analysis is very extensive. Only simple method of demagnetization is verified. Nonlinearity and temperature increase are not considered in the simulation.

The results of all simulations show correct procedure in the design and construction of the analysed machine. From results obtained in simulations the machine efficiency for both PM materials is



calculated. Values of efficiency are shown in Table 4.9. Low values of efficiency are given by wrong vector control of machine in simulation. The method of control to maximum torque per stator current is not used. That means the values of steady torque are not maximal for selected current. For all simulation is input current set equally.

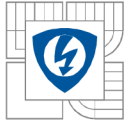
In last chapter of this thesis the optimization is performed with using Maxwell optimization module in first step, and then manually. Optimization in Maxwell was not successful because of the wrong settings. Optimization result given by generic algorithm is shown in Fig 39, where the body of PM is shown. Wrong setting resulted to minimalizing of cogging torque but wrong dimensions of the magnet. With this shape the magnet are susceptible to demagnetization on the sides.

For that reason manually optimization is performed. Four variations of magnet dimensions are selected, all variants with comparison to original machine is shown in Table 6.1. For each variant the values of steady torque and losses are evaluated. From simulations results the machine efficiency of optimized design is calculated in Table 7.1.

By performing of the simple optimization, the increase of machine efficiency is attained by 3,3%. Comparison of steady torque values for original and optimized design is shown in Table 7.2. Steady torque value is increased by 1,6 Nm.

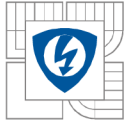
The aim of this thesis is to authenticate the possibilities of using Ansoft Maxwell for simulation and optimization of electrical machines. All simulations are finished correctly. Results are compared to analytically calculated values and results from other simulations software's. With created parametric model of machine the optimization of PM dimensions is done.

Ansoft Maxwell offers five different methods in optimetrics module. The simple task can be easily solved by these methods. Complex optimization task as the machine efficiency need results from several different simulations. Set Optimization goal to each simulation correctly is very complicated. For that reasons often the external programmes are used, for example Matlab. Optimization task is set in Matlab. Matlab starts simulations in Maxwell and evaluate the results. Machine efficiency is subsequently calculated in Matlab. With this software combination the much more complicated optimizations tasks can be solved easily and faster than piecewise in Maxwell.

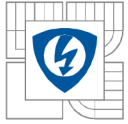


References

- [1] DUAN, Y. ; , “*Method for design and optimization of surface mount permanent magnet machines and induction machines*”. Georgia, 2010. Dissertation. Georgia Institute of Technology Supervisor: Harley, R. Available from: <http://hdl.handle.net/1853/37280>. Supervisor: Harley, R.
- [2] OUYANG, Wen, Damir ZARKO and T.A. LIPO. “Permanent Magnet Machine Design Practice and Optimization”. *Conference Record of the 2006 IEEE Industry Applications Conference Forty-First IAS Annual Meeting*. IEEE, 2006, p. 1905-1911. DOI: 10.1109/IAS.2006.256796. Available from: <http://ieeexplore.ieee.org/lpdocs/epic03/wrapper.htm?arnumber=4025484>
- [3] BIANCHI, N., S. BOLOGNANI and P. FRARE. “Design Criteria for High-Efficiency SPM Synchronous Motors”. *IEEE Transactions on Energy Conversion*. IEEE, 2006, vol. 21, issue 2, p. 396-404. DOI: 10.1109/TEC.2005.853720. Available from: <http://ieeexplore.ieee.org/lpdocs/epic03/wrapper.htm?arnumber=1634586>
- [4] DUAN, Y., R.G. HARLEY and T.G. HABETLER. “Method for multi-objective optimized designs of Surface Mount Permanent Magnet motors with concentrated or distributed stator windings”. *2009 IEEE International Electric Machines and Drives Conference*. IEEE, 2009, vol. 21, issue 2, p. 323-328. DOI: 10.1109/IEMDC.2009.5075225. Available from: <http://ieeexplore.ieee.org/lpdocs/epic03/wrapper.htm?arnumber=5075225>
- [5] MI, C.C. “Analytical design of permanent-magnet traction-drive motors”. *IEEE Transactions on Magnetics*. 2006, vol. 42, issue 7, p. 1861-1866. DOI: 10.1109/TMAG.2006.874511. Available from: <http://ieeexplore.ieee.org/lpdocs/epic03/wrapper.htm?arnumber=1644903>
- [6] BIANCHI, Nicola. “*Electrical machine analysis using finite elements*”. Boca Raton, FL: Talor, c2005. 275 p. ISBN 08-493-3399-7.
- [7] MISSOUM, R., N. BERNARD, M. E. ZAIM and J. BONNEFOUS. “Optimization of high speed surface mounted permanent magnet synchronous machines”. *2007 International Aegean Conference on Electrical Machines and Power Electronics*. IEEE, 2007, p. 446-451. DOI: 10.1109/ACEMP.2007.4510541. Available from: <http://ieeexplore.ieee.org/lpdocs/epic03/wrapper.htm?arnumber=4510541>
- [8] RAHMAN, M.A., P. ZHOU, M. E. ZAIM and J. BONNEFOUS. “Analysis of brushless permanent magnet synchronous motors”. *IEEE Transactions on Industrial Electronics*. IEEE, 2007, vol. 43, issue 2, p. 256-267. DOI: 10.1109/41.491349. Available from: <http://ieeexplore.ieee.org/lpdocs/epic03/wrapper.htm?arnumber=491349>
- [9] VAN DER VEEN, J.L.F., L.J.J. OFFRINGA a A.J.A. VANDENPUT. “Minimising rotor losses in high-speed high-power permanent magnet synchronous generators with rectifier load”. *IEE Proceedings - Electric Power Applications*. IEEE, 1997, vol. 144, issue 5, p. 331-. DOI: 10.1049/ip-epa:19971354. Available from: http://digital-library.theiet.org/content/journals/10.1049/ip-epa_19971354
- [10] YAO DUAN, M.A., R.G. HARLEY, T.G. HABETLER and J. BONNEFOUS. “A useful multi-objective optimization design method for PM motors considering nonlinear material properties”. *2009 IEEE Energy Conversion Congress and Exposition*. IEEE, 2009, vol. 43, issue 2, p. 187-193. DOI: 10.1109/ECCE.2009.5316144. Available from: <http://ieeexplore.ieee.org/lpdocs/epic03/wrapper.htm?arnumber=5316144>
- [11] DOSIEK, Luke, Pragasen PILLAY, T.G. HABETLER and J. BONNEFOUS. “Cogging Torque Reduction in Permanent Magnet Machines”. *IEEE Transactions on Industry Applications*. IEEE, 2007, vol. 43, issue 6, p. 1565-1571. DOI: 10.1109/TIA.2007.908160. Available from: <http://ieeexplore.ieee.org/lpdocs/epic03/wrapper.htm?arnumber=4384988>



- [12] ŠTULRAJTER, M., HRABCOVÁ, V., FRANKO, M.: "Permanents Magnets Synchronous Motor Control Theory. Journal of ELECTRICAL ENGINEERING", Vol.58, No. 2, 2007, p 79-84
- [13] CHEN, Y.S., Z.Q. ZHU, D. HOWE a J. BONNEFOUS. "Calculation of d- and q-axis inductances of PM brushless ac machines accounting for skew". *IEEE Transactions on Magnetics*. IEEE, 2005, vol. 41, issue 10, p. 3940-3942. DOI: 10.1109/TMAG.2005.854976.
Available from: <http://ieeexplore.ieee.org/lpdocs/epic03/wrapper.htm?arnumber=1519495>
- [14] Magnetic component Engineering. permanent magnets manufacturer [online]. [cit. 2012-12-05]. Available from: <http://www.mceproducts.com>
- [15] RUOHO, S., A. ARKKIO, D. HOWE a J. BONNEFOUS. "Partial Demagnetization of Permanent Magnets in Electrical Machines caused by an Inclined Field". *IEEE Transactions on Magnetics*. IEEE, 2008, vol. 44, issue 7, p. 1773-1778. DOI: 10.1109/TMAG.2008.921951.
Available from: <http://ieeexplore.ieee.org/lpdocs/epic03/wrapper.htm?arnumber=4544930>
- [16] SCHLIESCH, Lilly-Axinia. permanent magnets manufacturer [online]. [cit. 2012-12-05]. Available from: <http://www.permagsoft.com>
- [17] CHAITHONGSUK, Sisuda. "Design and construction of a permanent magnet synchronous motor (PMSM)". Bangkok, 2006. Master thesis. King Mongkut's Institute of Technology North Bangkok. Central Library. Supervisor: Nungam, S.
- [18] CHIN, Yung-Kang. "A permanent magnet synchronous motor for an electric vehicle: design analysis". Stockholm, 2004. ISBN 91-728-3803-5.
- [19] TJE MILLER. SPEED's Electric Machines: An outline of some of the theory in the SPEED software for electric machine design with problem and solutions. University of Glasgow, 2002-2009.
- [20] ANSYS INC. User's guide - Maxwell 2D: Electronic design automation software. Canonsbrug, 2010. Available from: <http://www.ansys.com>
- [21] URASAKI, N., T. SENJYU a K. UEZATO. "Influence of all losses on permanent magnet synchronous motor drives". *2000 26th Annual Conference of the IEEE Industrial Electronics Society. IECON 2000. 2000 IEEE International Conference on Industrial Electronics, Control and Instrumentation. 21st Century Technologies and Industrial Opportunities (Cat. No.00CH37141)*. IEEE, 2000, p. 1371-1376. DOI: 10.1109/IECON.2000.972321.
Available from: <http://ieeexplore.ieee.org/lpdocs/epic03/wrapper.htm?arnumber=972321>



Appendix A1 (material properties of steel M19_24)

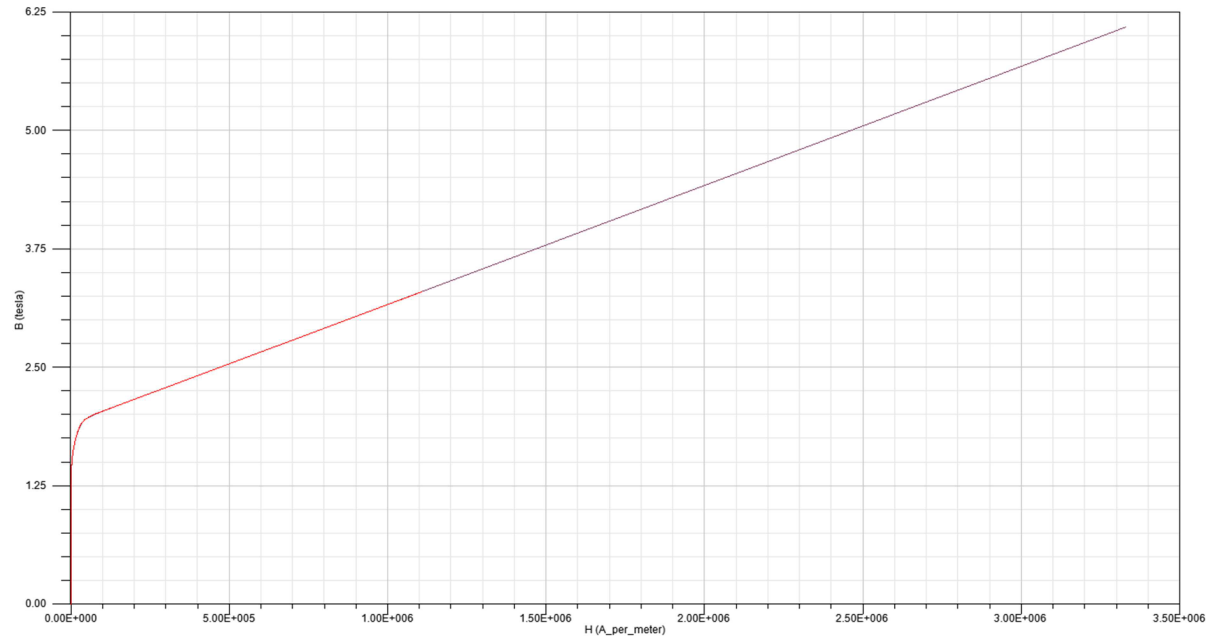


Fig 40.: BH curve of steel M19_24

Material Name: steel_M19_24gageLosses3
 Material Coordinate System Type: Cartesian

Properties of the Material

Name	Type	Value	Units
Relative Permeab...	Nonlinear	BH Curve...	
Bulk Conductivity	Simple	1950000	siemens/m
Magnetic Coercivity	Vector		
- Magnitude	Vector ...	0	A_per_me...
Core Loss Type		Electrical Steel	w/m^3
- Kh	Simple	213.117445931933	
- Kc	Simple	0.329630310163...	
- Ke	Simple	0	
- Kdc	Simple	0	
Mass Density	Simple	7650	kg/m^3

View/Edit Material for: Active Design, This Product, All Products

View/Edit Modifier for: Thermal Modifier

Validate Material

Calculate Properties for: [Dropdown]

Reset OK Cancel

Fig 41.: Properties of steel M19_24 in Maxwell

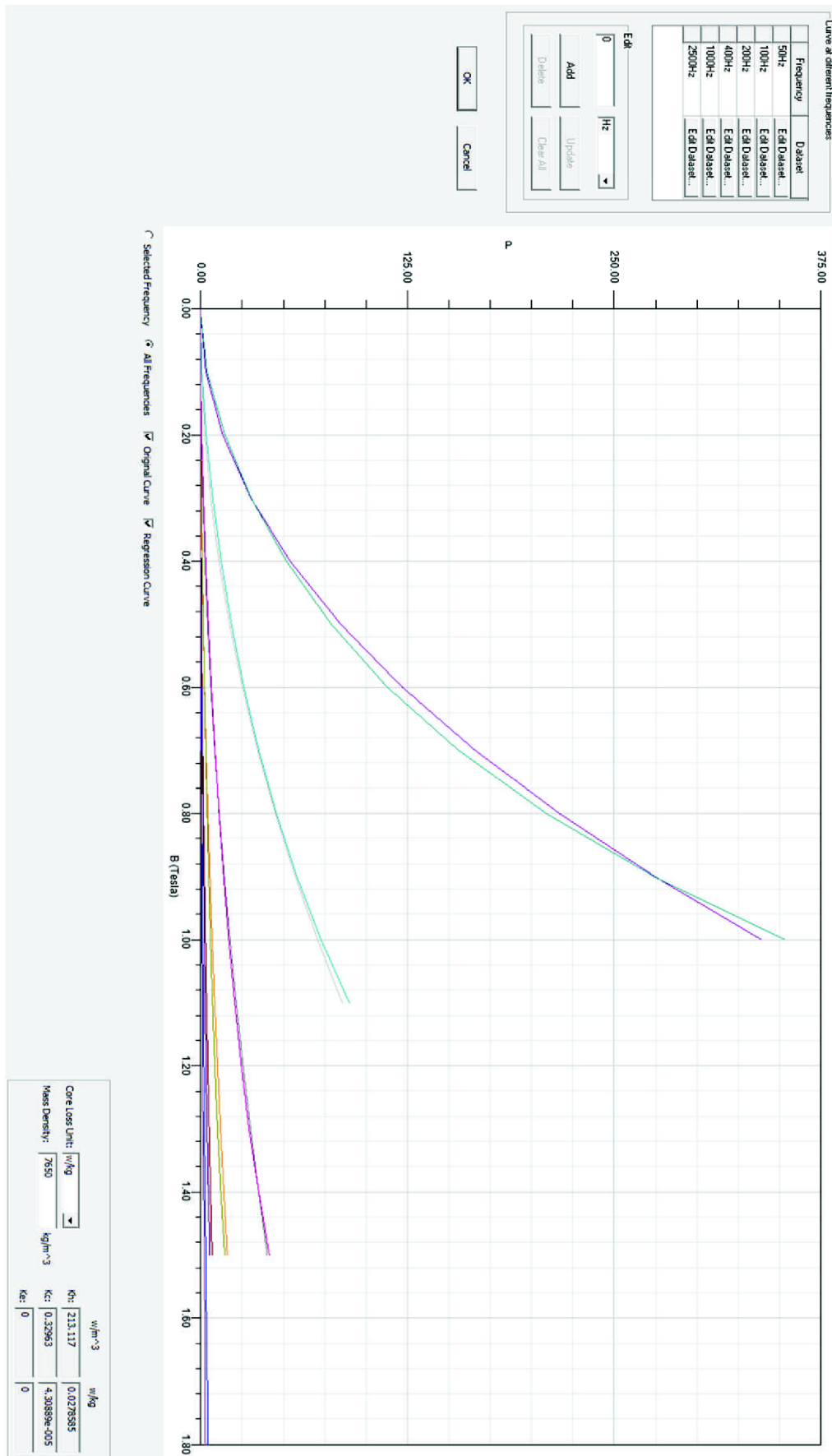
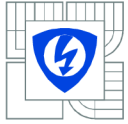
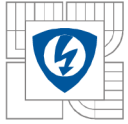


Fig 42.: Curves for calculation of core losses for steel M19_24 in Maxwell



Appendix B1 (material properties of NdFeB magnet)

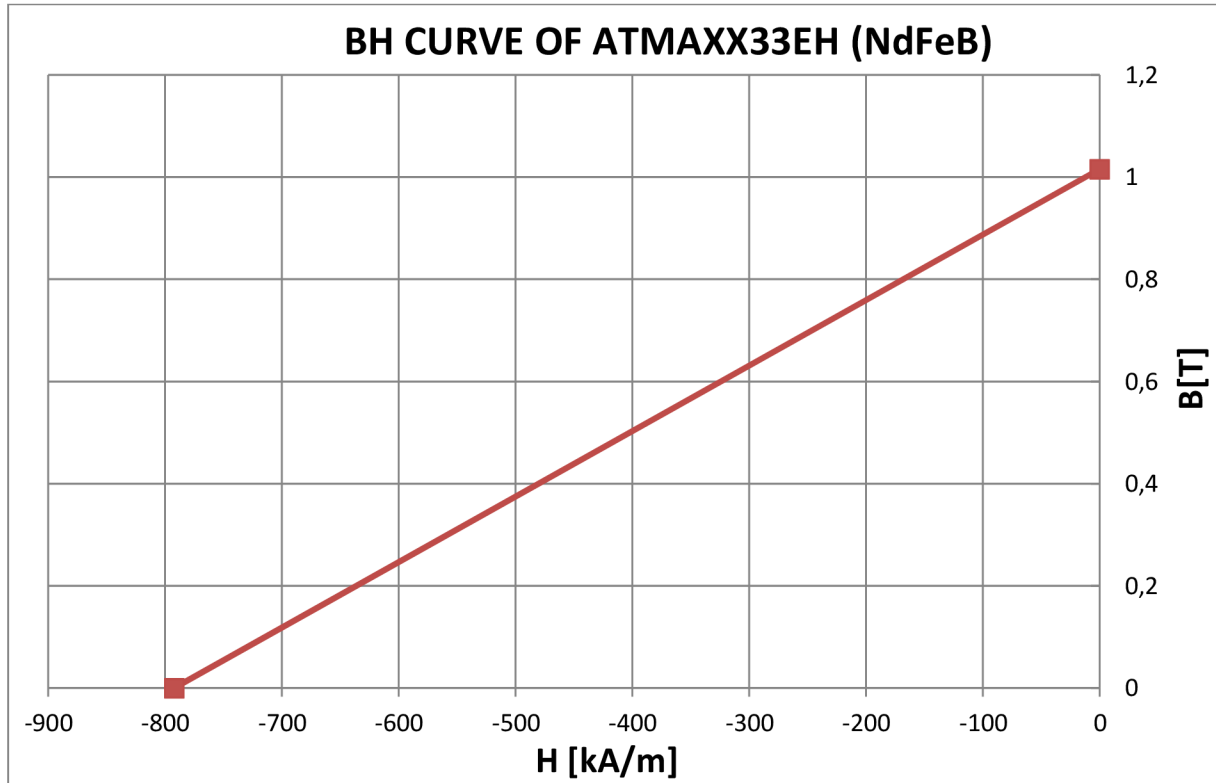


Fig 43.: BH curve of magnet material ATMAXX33EH

Material Name: SUMMITOMO_125C
Material Coordinate System Type: Cartesian

Name	Type	Value	Units
Relative Permeabi.	Simple	1.02	
Bulk Conductivity	Simple	625000	siemens/m
Magnetic Coercivity	Vector		
- Magnitude	Vector M...	-792263.9446559...	A_per_me...
- X Component	Unit Vec...	1	
- Y Component	Unit Vec...	0	
- Z Component	Unit Vec...	0	
Core Loss Type		None	w/m ³
Mass Density	Simple	7800	kg/m ³

View/Edit Material for:
 Active Design
 This Product
 All Products

View/Edit Modifier for:
 Thermal Modifier

Validate Material

Calculate Properties for: [Dropdown]

Reset OK Cancel

Mu: 1.02

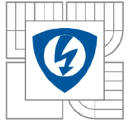
Hc: -792263.944655979 [A_per_meter]

Br/Mp

Br: 1.0155 [tesla]

Mp: 808109.223549099 [A_per_meter]

OK Cancel



Appendix C1 (material properties of SmCo magnet)

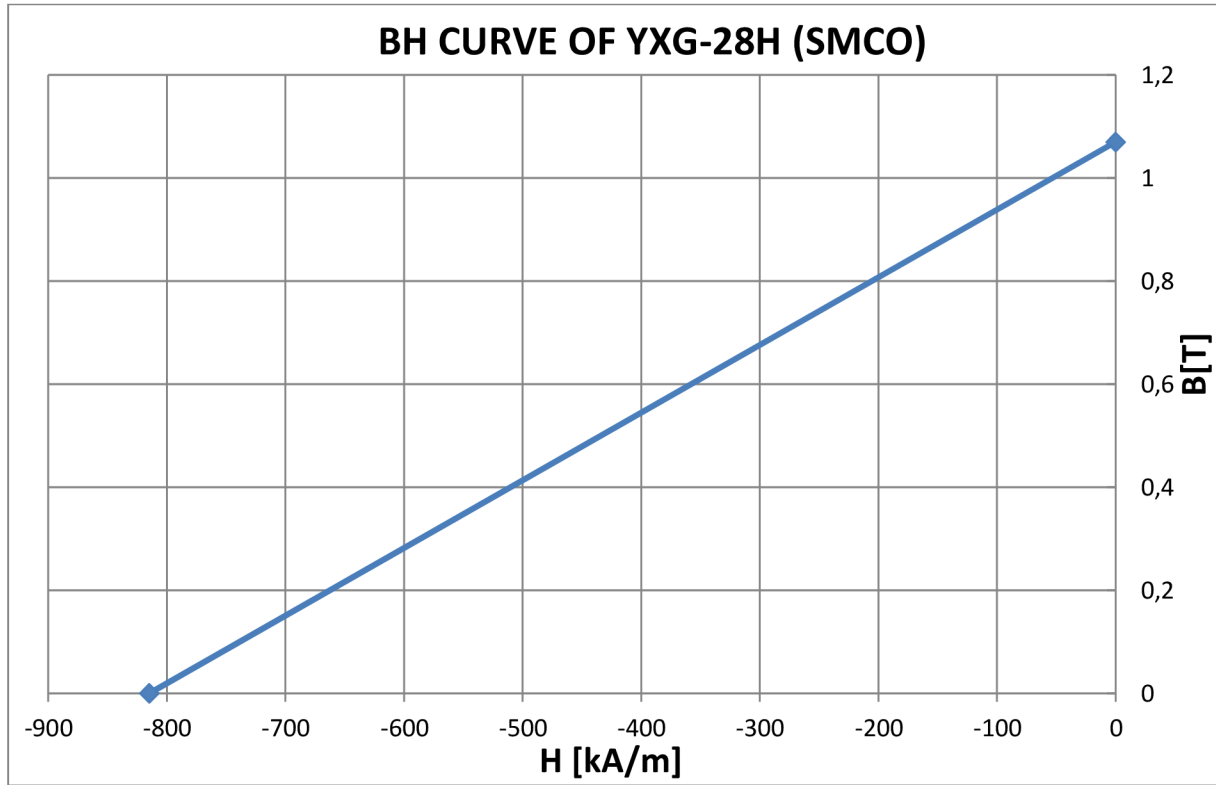


Fig 44.: BH curve of magnet material YXG-28H

Material Name: SmCo24_125C
 Material Coordinate System Type: Cartesian

Name	Type	Value	Units
Relative Permeabi...	Simple	1.049441968745...	
Bulk Conductivity	Simple	11111111	siemens/m
Magnetic Coercivity	Vector		
- Magnitude	Vector M...	-829714	A_per_me...
- X Component	Unit Vector	1	
- Y Component	Unit Vector	0	
- Z Component	Unit Vector	0	
Core Loss Type		None	w/m ³
Mass Density	Simple	8300	kg/m ³

View/Edit Material for:
 Active Design
 This Product
 All Products

View/Edit Modifier for:
 Thermal Modifier

Calculate Properties for: [dropdown]
 [Reset] [OK] [Cancel]

Mu: 1.04993129464246

Hc: -860933.000000003 [A_per_meter]

Br/Mp

Br: 1.1359 [tesla]

Mp: 903920.49929042 [A_per_meter]

[OK] [Cancel]